光学学报

手性光场及其在分子手性探测方面的近期研究进展（特邀）

穆晓伟，叶冲**，张向东*
北京理工大学物理学院，北京 100081

摘要 手性分子在自然界中广泛存在，探究手性分子的光学响应是一个热点问题。产生手性响应往往需要手性的光场，光场的手性很大程度上影响着手性介质的光学响应强度。因此，如何增强普通光场的手性特性是手性研究中的一个核心问题。通过合理设计微纳结构可以增强局域电磁场，使得分子与光场的相互作用增强，从而使得提高手性探测能力成为可能。本文主要围绕微纳结构超手性场的调制和在手性表征中的应用展开介绍，并聚焦近期的研究进展。一方面，本文介绍了基于微纳结构增强的超手性场；另一方面，介绍了基于超手性热点的手性分子超灵敏检测以及基于矢量外点的超手性场增强手性光力应用。除此之外，本文还介绍了合成手性光这一新型手性光场的相关研究，从手性光场的空间特征、光与分子相互作用和手性分子表征等方面比较手性光的差异。为更好地理解光场的手性以及分子手性光学响应的来源提供帮助，并且为进一步调控光场手性和利用它们实现更快、更准的手性分子表征提供新的思路。

关键词 微纳光学；超手性场；合成手性光
中图分类号 O436 **文献标志码** A **DOI**：10.3788/AOS231950

1 引 言

从星系的形状一直到原子核，手性在整个宇宙中无处不在。分子的手性作为手性的一个重要方面，由于其在生物、化学和药理等方面至关重要的作用而被广泛关注。不同手性的同种分子，互为手性对映体。分子手性的重要性可以追溯到生命的一个基本性质——“同手性”（homochirality）。生物体中所有的功能性氨基酸（蛋白质的组成部分）都是手性的，并且只有一种对映体存在生命体内。此外，它们在人类、动物、植物和细菌身上都具有相同的手性。糖也是如此，包括脱氧核糖，脱氧核糖也被称为DNA。不同的是，氨基酸都是左旋的，糖都是右旋的。这种生命在单一手性的基础上进化的趋势被称为“同手性”。生命的同手性被认为是实现高效的生命生物化学的必要机制，因此分子手性与生命的起源有着内在的联系[1]。

由于“同手性”以及化学反应和分子生物活性的手性依赖性，手性在药物安全等方面发挥着重要的作用。其中一个著名的例子与沙利度胺有关。沙利度胺的一种对映体可以有效缓解孕妇的晨吐，而另一种对映体则会导致严重的出生缺陷[2]。其他例子包括萘普生[3]、左旋多巴[4]、青霉胺[5]等。因此，手性分子的探测和提纯就显得极为重要。我们知道手性分子的两种对映体具有相同的熔点、沸点、密度等物理性质。要区别左右手分子，需要通过与其他物体相互作用。光作为人们研究最多的对象，自手性分子发现以来就在其探测和提纯上发挥着重要作用[6]。根据居里的不对称原则，产生手性响应往往需要手性的光场。当光场的某些性质，比如偏振和相位，具有空间结构并且和其镜像对称没办法通过平动和转动相互重合时，这样的光场就叫做手性光场。光场的手性程度影响着手性介质的光学响应强度。传统的手性光场是圆偏振光场，它在光旋转、圆二色性、拉曼光学活性和振动光学活性等手性响应中发挥着重要作用。然而，圆偏振光场产生的手性响应往往很弱，这极大影响了这些方法进行分子手性探测的能力。为了解决这个问题，人们提出了许多新的手性光场，比如超手性场（superchiral field）[7]、带轨道角动量（orbital angular momentum，OAM）的光场[8]和合成手性光场（synthetic chiral light）[9-15]，并研究了它们在手性分子表征上的重要应用[16-26]。

在本综述中，将主要围绕超手性场的调控，以及其在分子手性探测中的应用展开介绍。还将介绍合成手性光及其在手性探测等方面的应用，主要对比其在产生手性响应、自身的手性体现上与超手性场的差异。

收稿日期：2023-12-19；**修回日期**：2024-03-13；**录用日期**：2024-03-18；**网络首发日期**：2024-03-28
基金项目：国家自然科学基金（12105011）
通信作者：*zhangxd@bit.edu.cn；**yechong@bit.edu.cn

2 超手性光场及其在分子手性探测方面的应用

2.1 超手性光场

长期以来，人们一直认为，完全圆偏振的单色场具有最大的手性不对称性。然而在 2010 年 Tang 和 Cohen[7]提出了一种设置以获得不对称性超过圆偏振光的光场。具体地，他们提出利用两束手性相反、频率相等、强度略微不同的圆偏振的两个反向传播的平面波在光学驻波节点处实现增强的手性不对称性。他们将这样的光场，称为“超手性场”。场的手性强度可以利用 Lipkin's 00-zilch 密度[27]来量化，被 Tang 和 Cohen 称为“光学手性”（optical chirality），用“C”来表示，其表达式为

$$C=\frac{\varepsilon}{2}\boldsymbol{E}\cdot(\nabla\times\boldsymbol{E})+\frac{1}{2\mu}\boldsymbol{B}\cdot(\nabla\times\boldsymbol{B}),\tag{1}$$

式中：ε 和 μ 分别对应自由空间的介电常数和磁导率；$\boldsymbol{E}$ 和 $\boldsymbol{B}$ 为局部电场和磁场。光学手性也可以写为

$$C=-\frac{\varepsilon_0\omega}{2}\mathrm{Im}\left[\tilde{\boldsymbol{E}}(\boldsymbol{r})^*\cdot\tilde{\boldsymbol{B}}(\boldsymbol{r})\right],\tag{2}$$

式中，$\tilde{\boldsymbol{E}}$ 和 $\tilde{\boldsymbol{B}}$ 为复场的振幅[$\boldsymbol{E}=\mathrm{real}(\tilde{\boldsymbol{E}})$ 和 $\boldsymbol{B}=\mathrm{real}(\tilde{\boldsymbol{E}})$]。圆偏振光的光学手性 $C_0=\pm\frac{\varepsilon_0\omega|\boldsymbol{E}|^2}{2c}$，$c$ 为真空中的光速，这里的±表示入射圆偏振光的旋向。超手性场是比简单的左旋或右旋偏振光具有更高手性阶数的电磁场，其光学手性大于圆偏振光的光学手性（$C>C_0$）[28]。光场会引起手性分子的诱导电偶极矩 $\tilde{\boldsymbol{p}}$ 和诱导磁偶极矩 $\tilde{\boldsymbol{m}}$[29]：

$$\begin{cases}\tilde{\boldsymbol{p}}=\tilde{\alpha}_{\mathrm{ee}}\tilde{\boldsymbol{E}}-\mathrm{i}\tilde{\alpha}_{\mathrm{em}}\tilde{\boldsymbol{B}}\\ \tilde{\boldsymbol{m}}=\mathrm{i}\tilde{\alpha}_{\mathrm{em}}\tilde{\boldsymbol{E}}+\tilde{\alpha}_{\mathrm{mm}}\tilde{\boldsymbol{B}}\end{cases},\tag{3}$$

式中：$\tilde{\alpha}_{\mathrm{ee}}=\tilde{\alpha}'_{\mathrm{ee}}+\mathrm{i}\tilde{\alpha}''_{\mathrm{ee}}$、$\tilde{\alpha}_{\mathrm{em}}=\tilde{\alpha}'_{\mathrm{em}}+\mathrm{i}\tilde{\alpha}''_{\mathrm{em}}$ 和 $\tilde{\alpha}_{\mathrm{mm}}=\tilde{\alpha}'_{\mathrm{mm}}+\mathrm{i}\tilde{\alpha}''_{\mathrm{mm}}$ 是复数；$\tilde{\alpha}_{\mathrm{ee}}$ 是电极化率；$\tilde{\alpha}_{\mathrm{em}}$ 是各向同性混合电磁偶极子极化率；$\tilde{\alpha}_{\mathrm{mm}}$ 是磁化率。左旋圆偏振光和右旋圆偏振光的手性分子吸收速率 $Q_\pm$ 可以改写为以下形式[29]：

$$Q_\pm=\frac{\omega}{2}\left\langle\boldsymbol{E}\cdot\dot{\boldsymbol{p}}+\boldsymbol{B}\cdot\dot{\boldsymbol{m}}\right\rangle=\frac{\omega}{2}\mathrm{Im}\left(\tilde{\boldsymbol{E}}^*\cdot\tilde{\boldsymbol{p}}+\tilde{\boldsymbol{B}}^*\cdot\tilde{\boldsymbol{m}}\right)。\tag{4}$$

结合上面的式(3)和式(4)，可以得到

$$Q_\pm=\frac{\omega}{2}(\tilde{\alpha}''_{\mathrm{ee}}|\boldsymbol{E}|^2+\tilde{\alpha}''_{\mathrm{mm}}|\boldsymbol{B}|^2)\pm\tilde{\alpha}''_{\mathrm{em}}\mathrm{Im}(\tilde{\boldsymbol{E}}^*\cdot\tilde{\boldsymbol{B}})。\tag{5}$$

另外，结合式(2)，有 $Q_\pm=\frac{2}{\varepsilon_0}(\omega U_{\mathrm{e}}\tilde{\alpha}''_{\mathrm{ee}}-C^\pm\tilde{\alpha}''_{\mathrm{em}})$。$U_{\mathrm{e}}=\frac{\varepsilon_0}{4}|\tilde{\boldsymbol{E}}|^2$ 是时间平均电能密度。C^+ 和 C^-（$C^+=-C^-$）分别代表左旋和右旋圆偏振光激发的超手性场。则可以得到圆二色性（CD）谱信号，其定义为系统对等强度的左旋和右旋圆偏振光的吸收差，在下式中用 C_{D}[53,73]表示：

$$C_{\mathrm{D}}\propto Q_+-Q_-=-\frac{2}{\varepsilon_0}\tilde{\alpha}''_{\mathrm{em}}(C^+-C^-)\propto\Delta\hat{C},\tag{6}$$

式中，$\Delta\hat{C}=(C^+-C^-)/C_{\mathrm{CPL}}$ 对应于圆偏振光的超手性场。对于同一个圆偏振光，由于左右手分子的 $\tilde{\alpha}''_{\mathrm{em}}$ 互为相反数，可以定义能量交换的相对手性差异为

$$g\equiv 2\frac{Q_+^{\mathrm{L}}-Q_+^{\mathrm{R}}}{Q_+^{\mathrm{L}}+Q_+^{\mathrm{R}}}\propto\left(\frac{2C_+}{\omega U_{\mathrm{e}}}\right)。\tag{7}$$

除了能量交换以外，光学手性 C 也在手性光学梯度力中起到关键作用[30-32]。因此，通过研究光学手性就可以知道光场能产生手性响应的破缺程度。这为相关研究提供了极大的便利。

2.2 基于微纳结构增强的超手性近场

金属微纳结构支持的表面等离激元共振，不仅可以显著增强结构表面的电磁场强度，还可以增强超手性场，使光与手性分子作用大大增加，从而增强手性测量信号[33]。研究基于微纳结构的手性光场用于提升光学手性响应是一个热点[28,34-35]。早在 2010 年 Hendry 等[36]基于玻璃上的右手和左手 Gammadion 阵列构建了一种平面手性超材料，在近场区域以创建用于检测手性生物分子的手性等离子体热点。Schäferling 等[37]于 2012 年对 Gammadion 阵列的光学手性进行了测量和计算，发现在手性等离子体纳米结构的近场中可以形成具有强光学手性的电磁场。图 1(a)和 1(b)所示为考虑右旋圆偏振光和左旋圆偏振光作为入射光时，等离激元激发带来的近场超手性场。Meinzer 等[38]于 2013 年报道了手性金属等离子体结构与非手性分子结合来增强发光的手性不对称测量[图 1(c)上图和中图]，并计算了光学手性 C。他们观察到近场的不对称性超过了圆偏振光[图 1(c)下图]。

利用手性纳米结构增强 CD 谱、振动圆二色（VCD）谱以及拉曼光活性（ROA）谱等进行手性探测时[34]，分子的手性信号往往受到结构本身手性信号的影响。为解决这些问题，人们提出用非手性结构产生超手性光场实现增强的谱探测[39-48]。单个非手性纳米颗粒可以实现光学手性的局域增强[39]，然而采用银纳米球的研究发现，光学手性的增强并不均匀，整个空间的光学手性有正有负。高折射率介电纳米颗粒支持可见光和红外光谱中的电和磁共振[40-41]，可以实现光学手性的局域和全局增强。对于紧密堆积的纳米颗粒，可以在热点中产生强而均匀的超手性场。Liu 等[43]于 2015 年通过模拟表明，在非手性纳米颗粒二聚体的热点中存在由表面等离子体共振产生的超手性近场。Yao 等[42]于 2018 年通过电磁模拟研究了 Si 纳米立方体离散二聚体在圆偏振光或线偏振光激发下的近场手性，并证明了圆偏振光激发的强手性热点的形成。图 2(a)显示了二聚体间隙中会出现的手性热点，该热点始终与入射圆偏振光的手性具有相同的符号。

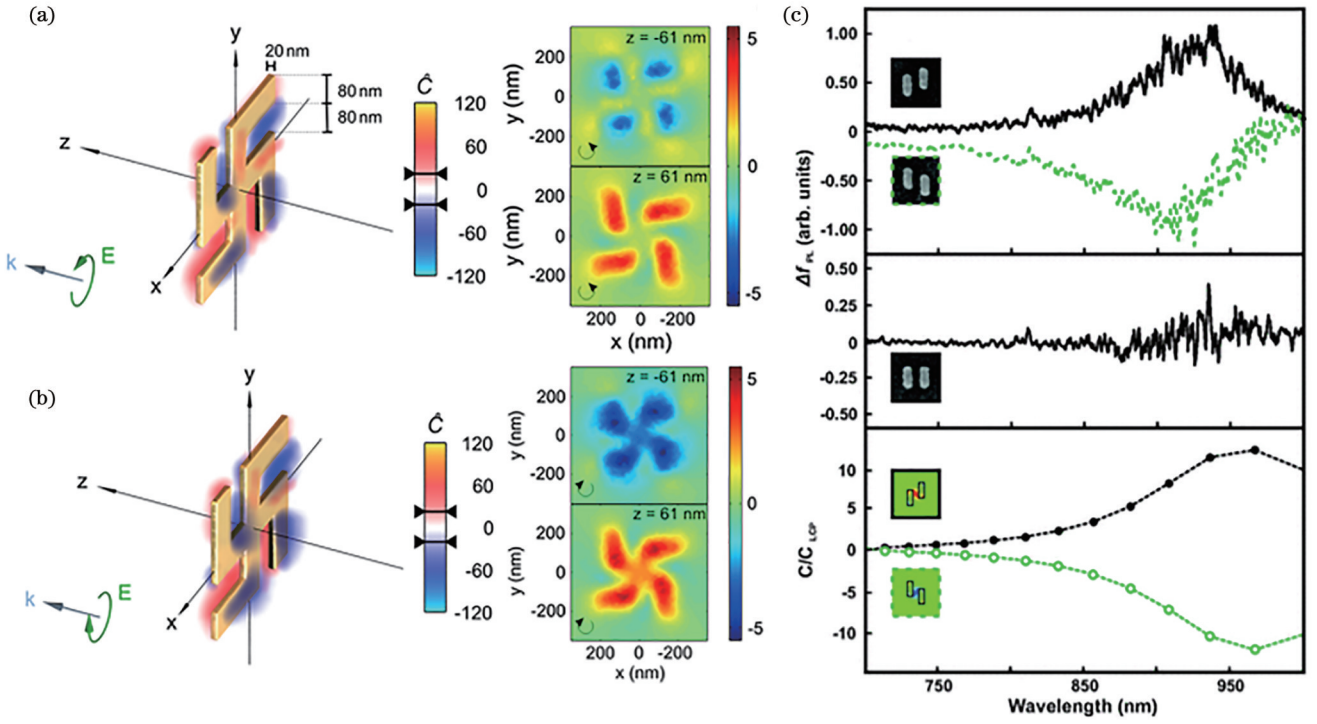

图 1 手性纳米结构产生的超手性光场。(a)、(b)用波长为 2.01 μm 的左旋圆偏振光和右旋圆偏振光照射平面 Gammadion 结构增强光学手性[37];(c)上图:对映体纳米棒对的两个阵列上左旋和右旋圆偏振光增强之间的不对称性。中图:等效纳米棒的非手性排列。下图:标准化电磁手性的有限元法(FEM)计算在纳米结构的纳米棒对上方 10 nm 的平面中的晶胞中心的手性光学密度。黑线代表左手,绿线代表右手[38]

Fig. 1 Superchiral optical field generated by chiral nanostructures. (a), (b) Optical chirality enhancement by a planar Gammadion structure illuminated with left circularly polarized light and right circularly polarized light at a wavelength of 2.01 μm[37]; (c) top picture: dissymmetry between left and right circularly polarized light enhancement on two arrays of enantiomeric nanorod pairs. Middle picture: an achiral arrangement of equivalent nanorods. Bottom picture: finite element method (FEM) for standardized electromagnetic chirality is used to calculate chiral optical density of crystal cell center in plane 10 nm above nanorod pairs in nanostructures. Black line represents left hand and green line represents right hand[38]

图 2(b)中黑色曲线显示了右旋圆偏振光照明(沿 z 轴传播)在二聚体间隙区域(70 nm×70 nm×10 nm)上平均的光学手性光谱。在 555 nm 处有一个明显的宽峰,增强因子超过 15 倍。高光学手性区域要求电场和磁场平行。这种情况在平面波中是不存在的,但是在倏逝的近场中可以实现。Zhao 等[44]于 2019 年通过电磁模拟和光谱学表征了线偏振光激发下对称硅纳米盘二聚体均匀符号近场手性的产生。如图 2(c)所示,硅纳米盘二聚体实现了 E 场和 H 场的平行排列,并且间隙区域中各自的场强度显著增强。

另外人们也研究基于非手性超材料在较大的区域上产生均匀且增强的手性场[45-47]。Wu 等[46]于 2020 年提出基于圆柱孔方形阵列的光子晶体板,构造矢量奇异点(vector EPs),以生成均匀超手性场。如图 2(d)所示,使用两束圆偏振光激励系统,在矢量 EP 点处产生超手性场。图 2(e)显示在矢量 EP 点处,出现最大光学手性(蓝线,厚度为 154.2 nm)。图 2(f)所示为矢量外点下,其本征模式的光手性密度 C 的近场分布,光子晶体板周围有符号相同的超手性场。

Zhang 等[48]于 2023 年提出利用矢量连续谱束缚态(BICs)构建超手性近场,并得到实验验证。通过调节 Si_3N_4 光子晶体板的厚度、孔直径等参数,在理论上设计了矢量 BIC 结构,将 TE 模式以及 TM 模式的 BIC 完美结合在一起,从而使光子晶体板附近的超手性场强度能够增强接近 1000 倍。图 2(g)和 2(h)显示了纳米孔直径的影响[图 2(g)中 d=145.5 nm,图 2(h)中 d=145 nm]的光子晶体板的能带结构,图 2(g)中插图显示了模式在 Γ 点周围相互叠加,表明矢量 BIC 的形成。图 2(h)插图表示 TE_B 和 TM_A 围绕 Γ 点的交叉点,称为矢量准 BIC。图 2(i)展示了这种准矢量 BIC 产生了三个数量级的手性场放大,并且整个光子晶体板的手性场都是均匀的。

2.3 基于超手性近场的手性分子的超灵敏检测

2.3.1 基于热点处超手性近场的手性分子超灵敏检测

在手性分子与单个金属纳米颗粒形成的手性纳米复合系统中实现增强的手性响应,通常受益于两方面:一方面是等离子诱导的手性分子内部电磁场变化;另

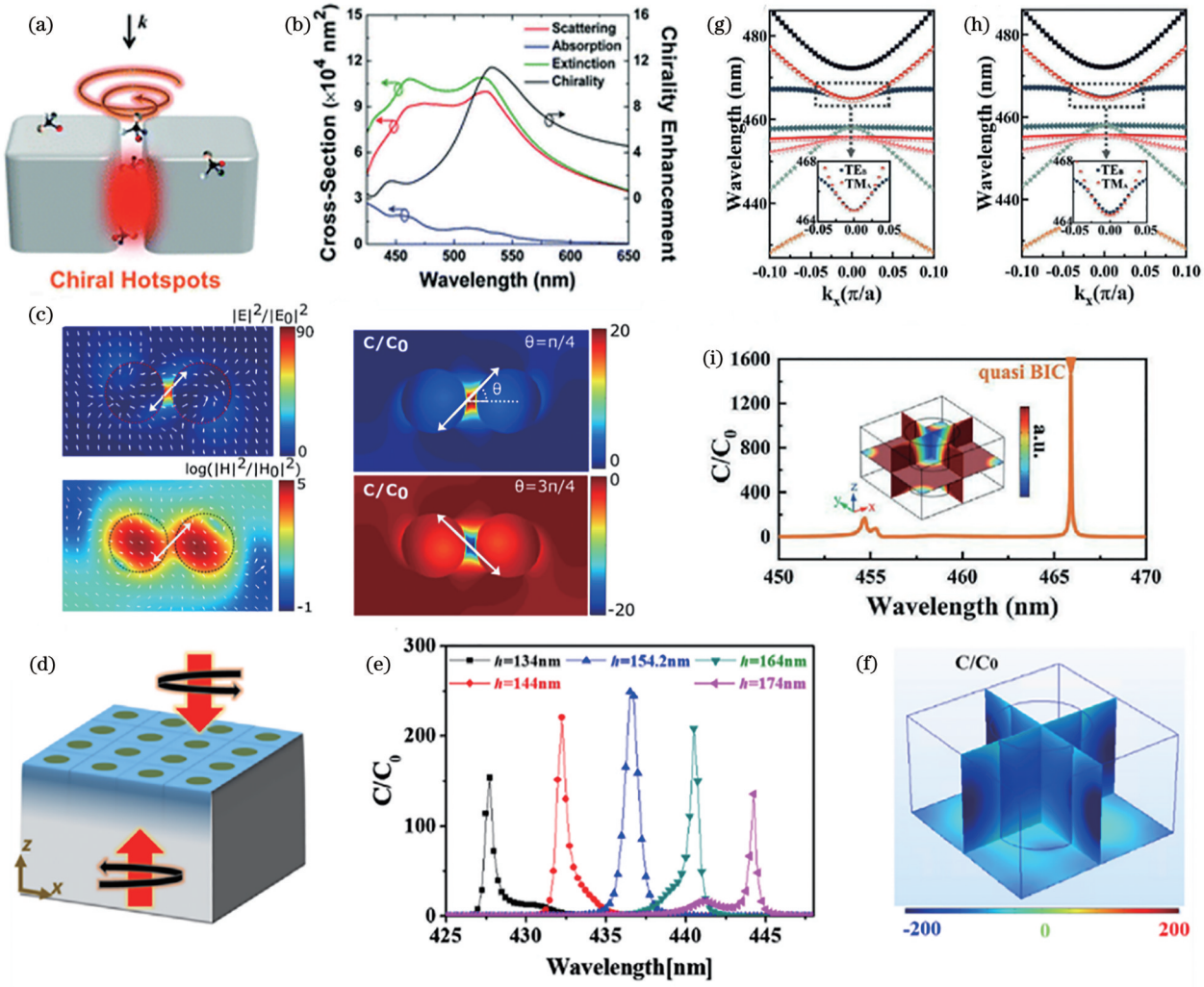

图 2 非手性纳米结构产生的超手性光场。(a)圆偏振光照射时,二聚体间隙中会出现手性热点(橙色模糊点);(b)右旋圆偏振光平面波顶部照射下二聚体间隙(黑色)的体积平均手性光谱以及二聚体散射(红色)、吸收(蓝色)和消光(绿色)横截面的光谱[42];(c)在 $\lambda=579$ nm 处,分离距离为 20 nm 的纳米盘二聚体的归一化 E 场和 H 场强度图,白色的小箭头表示向量场。入射线光偏振的方向由双头箭头给出(左二图)。在 $\lambda=140$ nm 处,硅纳米盘二聚体($D=100$ nm, $h=20$ nm, $g=579$ nm)的模拟光学手性增强,其中入射光角度 $\theta=\pi/4$和$3\pi/4$(右二图)[44];(d)使用从相反方向激励系统的两束圆偏振光在矢量 EP 处生成超手性场的方案;(e)具有不同厚度的圆柱形孔中的平均增强光学手性。蓝线对应于维持 EP 的结构,其中 $h=154.2$ nm。黑色、红色、绿色和粉色线对应于偏离矢量 EP 的情况;(f)在来自相反方向的两个激发光束下,在矢量 EP 处的光子晶体板附近的光学手性的近场分布[46];(g) $d=145.5$ nm 和(h) $d=145$ nm 的光子晶体板的能带结构。其他参数为 $a=270$ nm, $n_p=2.02$, $n_s=n_b=1.47$ 和 $t=154$ nm。插图显示了 TE_B 和 TM_A 在 Γ 点扩大的能带结构;(i) Si_3N_4 光子晶体板的手性场增强。参数为 $a=270$ nm, $h=154$ nm, $n_s=n_b=1.47$, $d=145$ nm, $k=0.0276$ rad/m[48]

Fig. 2 Superchiral light field generated by non chiral nanostructures. (a) Chiral hotspots (orange blurry spots) appear in gaps between dimers under circularly polarized light irradiation; (b) volume average chirality spectrum of dimer gaps (black) under top irradiation of right circularly polarized light plane waves, as well as spectra of dimer scattering (red), absorption (blue), and extinction (green) cross-sections[42]; (c) normalized E- and H-field intensity maps for dimers of nanodisks with separation of 20 nm at $\lambda=579$ nm. White arrow represents vector field and direction of polarization of incident light is given by a double headed arrow (two pictures on the left). Simulated optical chirality enhancement for Si nanodisk dimers ($D=100$ nm, $h=20$ nm, $g=579$ nm) at $\lambda=140$ nm with an incident light angle of $\theta=\pi/4$ and $3\pi/4$ (two pictures on the right)[44]; (d) scheme to generate superchiral field at vector EP using two beams of circularly polarized light exciting system from opposite directions; (e) average enhanced optical chirality in cylindrical pores with different thicknesses. Blue line corresponds to structure sustaining EP with $h=154.2$ nm. Black, red, green, and pink lines correspond to cases deviating from vector EP; (f) near-field distribution of optical chirality near photonic crystal slab at vector EP under two beams of excitation from opposite directions[46]; band structures of photonic crystal plates for (g) $d=145.5$ nm and (h) $d=145$ nm. Other parameters are $a=270$ nm, $n_p=2.02$, $n_s=n_b=1.47$, and $t=154$ nm. Illustration shows band structures of TE_B and TM_A expanding at point Γ; (i) chiral field enhancement of Si_3N_4 photonic crystal plates with parameters $a=270$ nm, $h=154$ nm, $n_s=n_b=1.47$, $d=145$ nm, and $k=0.0276$ rad/m[48]

一方面是由于纳米粒子和分子复合物的光吸收[22]。但是多纳米粒子系统相比于单纳米粒子系统产生的手性光学响应有更明显的增强。其原因除了等离子体耦合形成手性实体外[49]，还有多纳米粒子系统的热点效应。特定波长的入射光和金属纳米粒子相互作用时，可以激发局域表面等离子体共振(LSPR)，将纳米结构表面上的电场集中在非常小的点(热点)上，实现比单纳米颗粒强几个数量级的局部场增强。这些热点本质上像是集中光场的“透镜”。将手性分子放置于热点处，可以显著增强手性分子的光学响应。较大的手性光学效应与等离子体手性纳米结构有关[30]，可以通过改变团簇的大小、几何形状和相对于彼此的空间排列等来调节等离子体纳米结构的光响应并增强其光学不对称性(g因子)。

Markovich课题组[50]于2008年最早通过实验验证了分子附着在金属纳米粒子表面可以实现信号两个数量级的增强。而Govorov等[22]于2011年报道了等离子体二聚体可以有效地将电磁场集中到间隙区域，实现比单纳米颗粒强几个数量级的局域近场增强。如图3(a)显示了使用银二聚体的情况，对于小于光波长的颗粒间分离，CD信号得到了强烈的增强。在这种情况下，二聚体根据分子跃迁诱导CD的增强，并进一

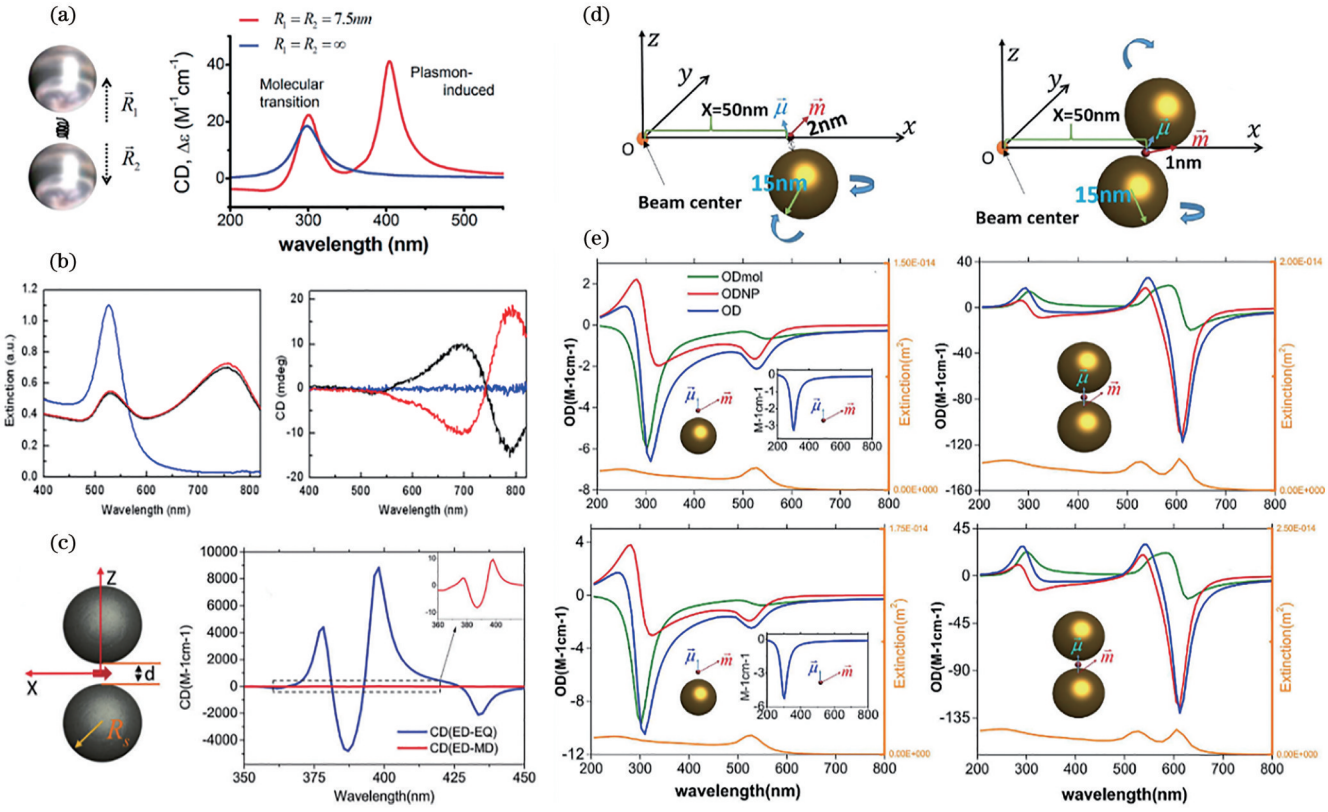

图3 基于热点处超手性近场的手性分子超灵敏检测。(a)示意图显示一个纳米颗粒二聚体在间隙中产生一个强局部的电磁热点，在这里手性分子可以经历与光的增强相互作用[22]；(b)分立的金纳米球颗粒(蓝色实线)、L-半胱氨酸修饰的金纳米球(黑线)和R-半胱氨酸修饰的金纳米球(红线)的消光光谱(左)和CD光谱(右)[23]；(c)由银二聚体和手性分子组成体系的示意图。纳米颗粒的半径设为$R_s=15$ nm(左图)，以及系统的CD(ED-EQ)和CD(ED-MD)随波长的函数。插图：CD(ED-MD)为360～400 nm(右图)[24]；(d)由金纳米颗粒(左图)、金二聚体(右图)和手性分子组成的复合物的坐标和示意图系统；(e) OAM入射光束的拓扑核分别为$l=\pm1$和$l=\pm2$时，单个手性分子和金纳米颗粒(左二图)和金二聚体(右二图)复合系统局域OD信号随波长的变化。插图表示没有纳米颗粒的单个手性分子的计算结果[63]

Fig. 3 Ultra sensitive detection of chiral molecules based on near field superchirality of hotspots. (a) Schematic diagram shows that a nanoparticle dimer generates a strong local electromagnetic hotspot in gap, where chiral molecules can undergo enhanced interactions with light[22]; (b) extinction spectra (left) and CD spectra (right) of discrete gold nanospheres (blue solid line) and L-GNSs (black line) and D-GNSs (red line)[23]; (c) schematic of system consisting of a Ag dimer and a chiral molecule. Radius of nanoparticles is set to $R_s=15$ nm (left figure). CD (ED-EQ) and CD (ED-MD) of system as functions of wavelength (inset: CD (ED-MD) is from 360 to 400 nm) (right figure)[24]; (d) coordinate and schematic diagram system of a complex composed of gold nanoparticles (left figure), gold dimers (right figure), and chiral molecules; (e) local OD signal as a function of wavelength for composite system of single chiral molecule and gold nanoparticles (two pictures on the left) and gold dimer (two pictures on the right) under OAM incident beams with $l=\pm1$ and $l=\pm2$, respectively. Insets represent calculated results for single chiral molecule without nanoparticles[63]

步在银纳米颗粒的共振频率下产生等离子体诱导的CD峰。Layani等[51]于2013年讨论了电磁热点在小聚集体中银纳米颗粒之间的间隙中的重要性，他们仅在聚集状态下观察到CD效应；在分离纳米颗粒后，强热点消失，效应消失。纳米颗粒热点的进一步控制可以通过改变其形状来实现。例如，在银纳米立方体的情况下，热点出现在顶点处[52]。

Wang等[23]于2014年在实验上制备了半胱氨酸为媒介的金纳米颗粒(GNSs)线性装配的三聚体。通过实验观察到位于金纳米球团簇热点的半胱氨酸(Cys)分子在可见光区域的CD增强约为两个数量级。图3(b)曲线分别表示分立的金纳米球(蓝线)、L-半胱氨酸修饰的金纳米球(L-GNSs，黑线)和R-半胱氨酸修饰的金纳米球(D-GNSs，红线)的消光光谱和相应的CD谱。由于线性结构中相邻粒子之间的强近场等离子体耦合，在较长的波长侧出现了新的等离激元共振。由于在未添加Cys分子的情况下，GNSs胶体溶液中没有检测到CD信号[图3(b)中的蓝色实线]，因此L-GNSs或D-GNSs簇中的强烈CD响应与热点处Cys分子存在密切相关。

大部分电四极子(EQ)的贡献通常被认为相对较小且被忽视。最近一些实验现象表明EQ在一些光学响应中起着关键作用[24,26,54-56]。与偶极近似的情况不同，分子EQ相关的等离子体CD活性主要出现在等离子体共振吸收处，等离子体共振吸收促进了光学增强近场，Wu等[24]于2017年研究了各种纳米复合材料对等离子体诱导的CD信号的EQ贡献。特别是，对于具有优先分子取向且位于等离子体纳米结构热点的手性介质，EQ贡献的等离子体CD强度可以比分子电/磁偶极子贡献的等离子体CD强度高两个数量级。图3(c)显示了放置在银二聚体热点中的手性分子(两个银球半径为15 nm，间距为1 nm)(左图)，以及手性分子的电偶极子(ED)和磁偶极子(MD)相互作用引起的CD信号[CD(ED-MD)]和电四极子的贡献[CD(ED-EQ)](右图)。在$\lambda=398$ nm时，CD(ED-EQ)的值约为峰值时[CD(ED-MD)]的1000倍。当纳米颗粒数量逐渐增加时，会表现出不一样的性质。并且金属团簇结构的对称性对热点处分子手性响应也有影响。Zhang等[33]于2017年计算了大量定向分子的等离激元增强CD信号。结果表明，等离子体诱导的CD对分子的取向很敏感。在许多情况下，分子电四极矩跃迁对总CD信号的贡献可以起关键作用。并且证明，通过匹配电磁场的相位及其在纳米结构周围不同区域的近场梯度，可以大大改善基于电四极矩和偶极子的CD信号。

除此之外，轨道角动量(OAM)光束和手性分子之间相互作用的问题被人们广泛讨论[57-63]。Wu等[63]于2015年研究了OAM光束与手性分子-纳米颗粒团簇之间的相互作用，发现单个纳米球颗粒对OAM失谐(OD)谱的增强很小，而当将手性分子置于二聚体的热点中时，可以观察到巨大的增强效应。图3(d)表示由金纳米颗粒、金纳米二聚体和手性分子组成的复合物。图3(e)给出单个金纳米颗粒以及金纳米二聚体的OD和消光随波长变化的函数。与纯手性分子的OD谱[图3(e)插图]相比，发现金纳米颗粒和手性分子复合物光谱在$\lambda=300$ nm附近的OD_{mol}信号提高了约2倍。与单球的情况相比，金纳米二聚体在耦合等离子体共振波长附近的总OD值显著增强。

相比于CD谱，ROA谱能够给出更全面的分子手性结构相关的信息，但通常ROA信号很小，实验上很难去测量。另外人们一直认为磁场很难增强分子的表面增强拉曼光活性(SEROA)谱[64-65]。最近的研究表明，由于纳米粒子附近的大磁场、增强的分子磁偶极子辐射以及纳米粒子的磁偶极子响应引起的电场对称破坏，硅纳米粒子可以显著增强ROA信号[26]。Wu等[26]于2016年研究了纳米结构与各向异性手性分子材料之间的电磁相互作用，利用介电纳米颗粒增强分子ROA信号。对于Si和Au纳米颗粒二聚体，当分子置于热点时，由于热点处强烈的近场电磁场局域效应，尽管这两种系统的SEROA信号几乎相同，但Si纳米颗粒二聚体的信噪比可以比Au二聚体大60倍。图4(a)即为不同间距的Si纳米球二聚体以及Au纳米球二聚体系统热点处的SEROA信号，可以观察到典型的等离子体增强峰。

Zhang等[66]于2017年讨论了位于间隙纳米天线热点的手性分子(介质)的近场手性光学放大效应。Si纳米二聚体可以诱导比Au纳米二聚体更大的CD信号。此外，介电结构在光照射时热效应相比于金属结构更小。图4(b)讨论了基于Si(黑线)和Au(红线)纳米二聚体的增强型CD的光谱、手性光密度和消光光谱。可以明显看到，硅基纳米二聚体同时发生电共振和磁共振，Si基纳米粒子的CD增强总是比金基等离子体粒子强。图4(c)表示了Si(黑色虚线)和Au(红色虚线)纳米球周围的温度随波长变化的情况。黑色和红色箭头标记了Si和Au纳米二聚体诱导的CD峰的位置。显然，Si纳米二聚体是一种更好的纳米天线，具有超低的热量来增强CD信号。

有些纳米粒子既可以增大手性分子的光学响应，又可以产生固有的光学信号[36,67-72]。Wu等[25]于2014年研究了金纳米颗粒与手性分子的近场等离子体耦合由于旋转和位移导致的结构CD信号。将手性分子置于手性结构的热点中，纳米颗粒位错引起的球状三聚体中分子诱导的等离激元手性完全被结构手性所抑制，总的CD信号并不能反映分子手性的信息。图4(d)表示金纳米颗粒旋转引起的球状三聚体手性结构的CD信号。对于这种情况，结构CD信号在分子诱导的CD信号的波长处(650 nm)较弱，因此可以从CD光谱中检测手性分子的手性。传统光谱测量中系

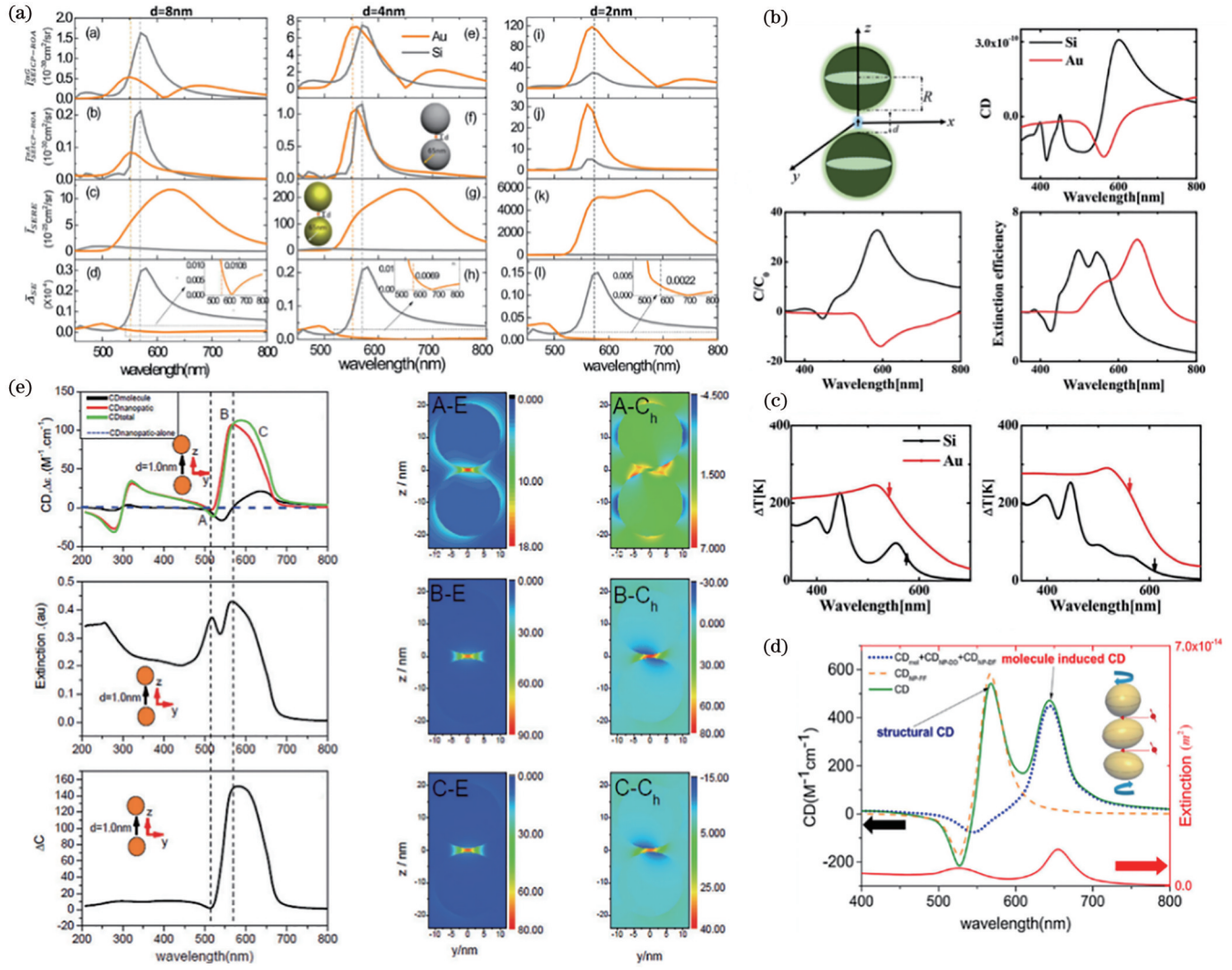

图 4　基于热点处超手性近场的手性分子超灵敏检测。(a)分别在 $d=8$ nm，$d=4$ nm 和 $d=2$ nm 处的 SEROA 谱的 $\tilde{\alpha}\tilde{G}$ 分量（$\bar{I}^{\alpha G}_{(\mathrm{SE})\mathrm{ICP\text{-}ROA}}$）、平均 $\tilde{\alpha}\tilde{A}$（$\bar{I}^{\alpha A}_{(\mathrm{SE})\mathrm{ICP\text{-}OA}}$）、模式平均表面增强或未增强的拉曼散射强度（$\bar{I}_{(\mathrm{SE})\mathrm{RS}}$）以及模式平均圆形强度差 $\bar{\Delta}_{\mathrm{SE}}$[26]；(b)由手性分子和纳米球组成的杂化系统的几何形状和坐标。手性分子被置于坐标的原点。半径为 R 的纳米球位于 R_s。Si（黑线）、Au（红线）单纳米球（左）和二聚体（右）增强的 CD 谱、手性光学密度和消光光谱；(c) Si（黑线）、Au（红线）单纳米球（左）和二聚体（右）体系的温度增量随波长的变化[66]；(d)计算了由 $a=17.5$ nm、$b=17$ nm、$\alpha_p=0.0025°$、间隙为 1 nm 的旋转纳米粒子引起的金球形三聚体手性结构的 CD 和消光随波长的变化。实线、虚线和点线分别表示总 CD、结构手性（$\mathrm{CD}_{\mathrm{NP-FF}}$）和分子诱导的等离子体手性（$\mathrm{CD}_{\mathrm{mol}}+\mathrm{CD}_{\mathrm{NP-DD}}+\mathrm{CD}_{\mathrm{NP-DF}}$）；红线表示消光[25]；(e)金纳米球二聚体与分子复合体系的 CD 信号、对应的消光光谱以及超手性场随波长的变化。A-E、B-E 和 C-E 表示在左旋圆偏振光激发下，y-z 平面上 A、B 和 C 点的电场分布，$\mathrm{A-C_h}$、$\mathrm{B-C_h}$ 和 $\mathrm{C-C_h}$ 是相应的光学手性[43]

Fig. 4　Ultra sensitive detection of chiral molecules based on near field superchirality of hotspots. (a) $\bar{I}^{\alpha G}_{(\mathrm{SE})\mathrm{ICP\text{-}ROA}}$, average $\tilde{\alpha}\tilde{A}$ ($\bar{I}^{\alpha A}_{(\mathrm{SE})\mathrm{ICP\text{-}OA}}$), mode average surface enhanced or unenhanced Raman scattering intensity ($\bar{I}_{(\mathrm{SE})\mathrm{RS}}$), and corresponding surface enhanced mode averaged circular intensity differences $\bar{\Delta}_{\mathrm{SE}}$ of SEROA spectra at $d=8$ nm, $d=4$ nm, and $d=2$ nm, respectively[26]; (b) geometric shape and coordinate of a hybrid system composed of chiral molecules and nanospheres. Chiral molecules are placed at origin of coordinate. Nanosphere, with radius R, locates at R_s. Enhanced CD spectra, chiral optical densities, and extinction spectra of Si (black line), Au (red line) single nanospheres (left), and dimers (right); (c) temperature increment of Si (black line), Au (red line) single nanospheres (left), and dimer (right) systems as a function of wavelength[66]; (d) CD and extinction of chiral structure of gold spherical trimer induced by rotating nanoparticles with a gap of 1 nm are calculated as functions of wavelength. Parameters: $a=17.5$ nm, $b=17$ nm, $\alpha_p=0.0025°$. Solid line, dashed line, and dotted line represent total CD, structural chirality ($\mathrm{CD}_{\mathrm{NP-FF}}$), and molecular induced plasma chirality ($\mathrm{CD}_{\mathrm{mol}}+\mathrm{CD}_{\mathrm{NP-DD}}+\mathrm{CD}_{\mathrm{NP-DF}}$), respectively; red line represents extinction[25]; (e) CD signal of dimer and molecular composite system of gold nanosphere, corresponding extinction spectra, and superchiral fields as functions of wavelength. A-E, B-E, and C-E represent electric field distribution at points A, B, and C on y-z plane under left circularly polarized light excitation. $\mathrm{A-C_h}$, $\mathrm{B-C_h}$, and $\mathrm{C-C_h}$ are corresponding optical chiralities[43]

统总CD信号通常是分子诱导的CD信号和结构手性CD信号的结合。当结构手性CD信号远大于诱导产生的CD信号时，系统总CD信号虽然得到增强，但是很难反映手性分子信息。因此量化分子诱导的手性信号对来自纳米复合材料的整体CD信号的个体贡献对于手性探测极为重要。

过去人们认为将分子置于热点中手性信号显著增强是由于热点处的场强增强引起的。Liu等[43]于2015年证明热点中超手性场起着至关重要的作用。图4(e)显示了由手性分子和金二聚体组成的混合系统的CD、消光光谱和超手性场(金球的半径为10 nm，距离为1 nm)。可以看出CD信号和消光光谱不存在良好的对应关系，而超手性场始终对应于CD信号。这一点在右侧图中得到了印证。右侧图示为A、B和C点的电场强度和光学手性分布。由此可以确定，近场的光学手性而不是热点处的电磁场增强直接影响CD信号。这很好地解释了实验结果[图3(b)]，打破了热点的局部场强与等离子体诱导的CD强度直接相关的认知。

2.3.2 基于矢量外点构建超手性场提高手性检测灵敏度

除此之外，手性材料的电磁响应表现为不同的手性极化率，这为对映体分离提供了一种利用手性依赖的光力新方法[74-76,78-80]，其中作用在对映异构体上的手性光学力方向相反。而手性光学梯度力的强弱与光场手性的梯度有关[30,81-82]，利用超手性场可以增大对映体的总光力差[31-32,77,89]。

Liu等[31]于2022年基于不对称光子晶体板中的矢量奇异点，在不同时间改变入射光的相对相位，提出了一种实现分离纯化相反对映异构体的方法。在两束反向圆偏振光的激发下，在光子晶体板附近可以产生大的近场光学手性梯度，并且可以通过改变两束圆偏振光的相对相位来调节增强手性光力的方向，实现对映体的分离。图5(a)显示了作用在手性粒子上的每一项光力的贡献。如图5(b)所示，黑线、红线和蓝线对

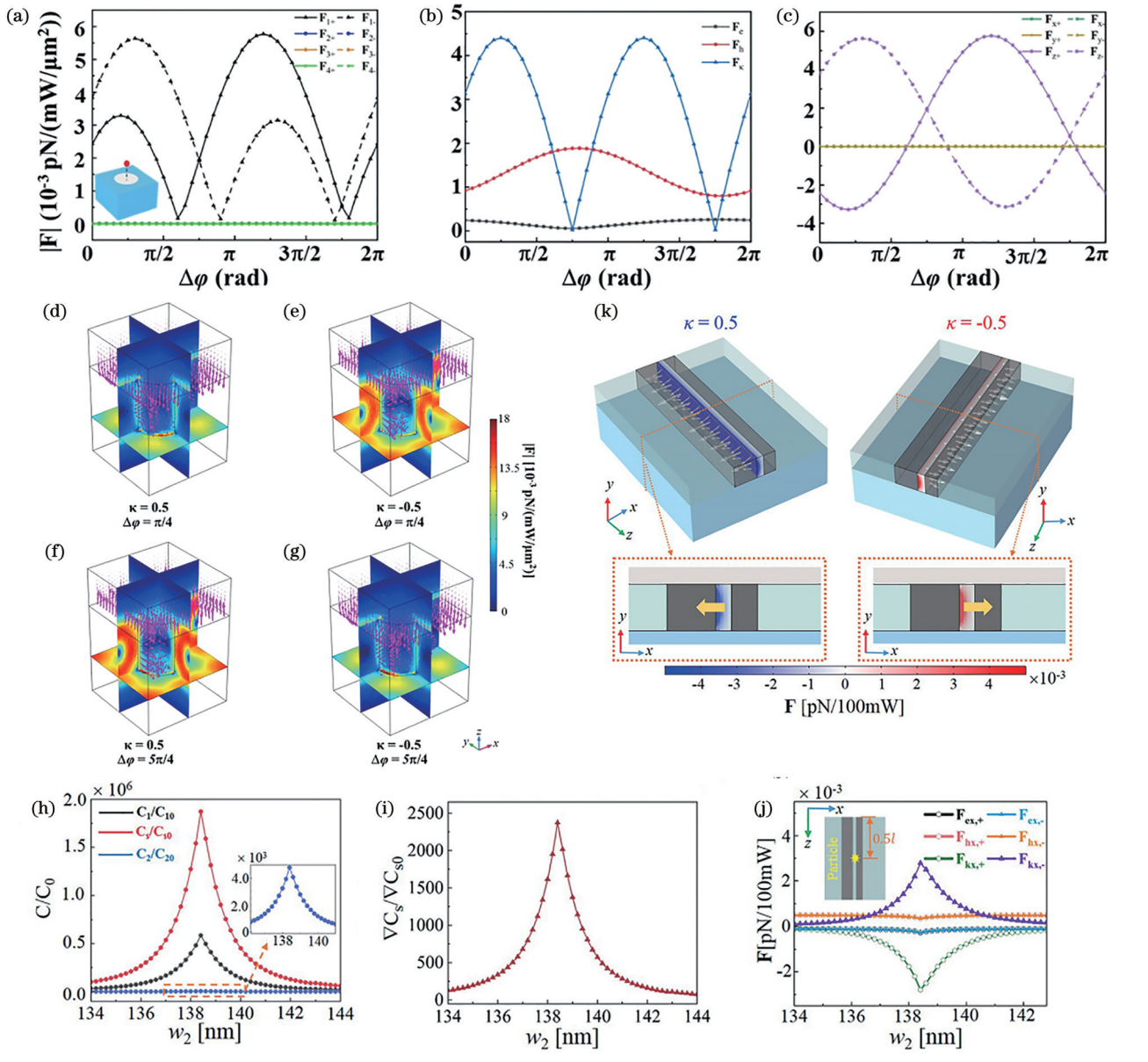

图 5 基于矢量外点构建超手性场的增强手性光力的应用。(a)作用在手性粒子上光力每一项的贡献。左下角的插图是手性粒子放置的示意图;(b)电场梯度力 F_e、磁场梯度力 F_h 和手性梯度力 F_k 的大小随相对相位的变化情况;(c)对映体($\kappa=+0.5$ 和 $\kappa=-0.5$)上沿 x、y、z 方向的光力分量随着入射光的相对相位而变化;(d)~(g)当相对相位分别为 $\pi/4$ 时,$\kappa=+0.5$ 和 $\kappa=-0.5$ 的情况下,光学力在三维空间中的强度分布和方向(用箭头标记)。当相对相位为 $5\pi/4$ 时,$\kappa=+0.5$ 和 $\kappa=-0.5$ 情况下的光学力分布[31];(h)手性场的空间平均增强随不同区域的宽度 w_2 的变化[臂 1(C_1/C_{10})、两个臂之间的槽(C_s/C_{s0})、臂 2(C_2/C_{20})]。这里,C_{i0} 表示不同区域在左右对称($w_2=256$ nm)情况下手性场的空间平均值;(i)缝隙通道中手性梯度场的空间平均增强随宽度 w_2 的变化;(j)沿着 x 轴的电场梯度力 F_e、磁场梯度力 F_h 和手性梯度力 F_k 随宽度 w_2 的变化。图中力的下标±表示手性参数 $\kappa=\pm0.5$。插图是手性粒子放置的示意图;(k)作用在缝隙通道中一对对映异构体 $\kappa=0.5$ 和 $\kappa=-0.5$ 上的光学力的强度分布和方向。插图显示了二维 x-y 平面中的相应力[32]

Fig. 5 Application of enhanced chiral optical force based on vector EPs to construct a superchiral field. (a) Contribution of each term of optical force on chiral particle. Bottom left illustration is schematic diagram of placement of chiral particle; (b) magnitude of electric field gradient force F_e, magnetic field gradient force F_h, and chiral gradient force F_k as a function of relative phase; (c) optical force component along x, y, and z directions on enantiomers ($\kappa=+0.5$ and $\kappa=-0.5$) changes with relative phase of incident light; (d-g) when relative phase is $\pi/4$, intensity distribution and direction of optical forces in three-dimensional space are indicated by arrows in case of $\kappa=+0.5$ and $\kappa=-0.5$. Optical force distribution under $\kappa=+0.5$ and $\kappa=-0.5$ conditions when relative phase is $5\pi/4$[31]; (h) spatially averaged enhancement of chiral field as a function of width w_2 for different regions [arm1(C_1/C_{10}), slot between two arms (C_s/C_{s0}), and arm1 (C_2/C_{20})]. Here, C_{i0} represents spatial average of chiral field in different regions under left-right symmetry ($w_2=256$ nm); (i) spatially averaged enhancement of chiral gradient field in slot channel as a function of width w_2; (j) electric field gradient force F_e, agnetic field gradient force F_h, and chiral gradient force F_k along x axis varying with width w_2. Subscripts ± of force in figure represent chiral parameters $\kappa=\pm0.5$. Illustration is a schematic diagram of placement of chiral particles; (k) intensity distribution and direction of optical forces acting on a pair of enantiomers with $\kappa=0.5$ and $\kappa=-0.5$ in a gap channel. Illustration shows corresponding forces in two-dimensional x-y plane[32]

应于计算出的 F_e、F_h 和 F_k 作为相对相位 $\Delta\varphi$ 的函数,可以清楚看出手性梯度力 F_k 起主导作用。图 5(c)计算了沿 x、y、z 轴的光力,注意到作用在 z 轴上的力远大于其他两个方向上的力,有助于在 z 方向捕获和分离手性粒子。图 5(d)、5(e)[或图 5(f)、5(g)]显示了当相对相位为 $\pi/4$(或 $5\pi/4$)时,作用在一对对映体($\kappa=0.5$)上的总光力的强度和方向分布。因此通过适当调整两束圆偏振光的初始相对相位,可以实现光力的手性选择性增强和开关效应,完成纳米粒子的对映体分离。

另外,最初设计的光子微纳结构[31,45,83-85]不允许在大面积上进行手性依赖性光学操作,这使得对映异构体的分离距离受到限制。基于不对称光子晶体板中的矢量奇异点,Liu 等[32]于 2023 年从理论上设计了一种硅基微流控芯片,实现手性纳米颗粒的高效分离。通过打破一对有损波导的镜面对称性,两个原始的正交模式相互耦合,触发矢量奇异点的形成。在矢量 EP 点的辅助下,微流控芯片可以产生超手性梯度场,引起极强的手性梯度力,将具有相反手性纳米颗粒推向延伸槽的不同侧面。图 5(h)表示不同区域[臂 1(C_1/C_{10},黑线)、两个臂间的槽(C_s/C_{s0},红线)、臂 2(C_2/C_{20},蓝线)]的手性场的空间平均增强,其中 $C_{i0}(i=1,s,2)$ 表示镜面对称结构不同区域的手性光场的空间平均值。可以看出,所有类型的近场都出现在不同的区域。特别是,缝隙(C_s)中手性光场的空间平均值提高了 2 个数量级。图 5(i)表示手性梯度获得了三阶的空间平均增强。图 5(j)计算了沿 x 轴的光学梯度力的每个分量(电场梯度力 F_{ex}、磁场梯度力 F_{hx} 和手性梯度力 F_{kx}),插图表示将手性纳米粒子(半径 $r_p=4$ nm)放入距入口 1 μm 的槽中。对于手性参数 $\kappa=0.5$ 和 $\kappa=-0.5$ 的粒子,F_x 的大小都远大于其他两个方向上的力。图 5(j)展示了手性梯度力 F_k 依赖于对映体的手性,在结构中起主导作用。图 5(k)为作用在对映体($\kappa=\pm0.5$)上的总光力的强度和方向的空间分布。其中插图清楚地表明,作用在 $\kappa=0.5$ 的纳米粒子上的光力方向与 $\kappa=-0.5$ 时相反。

3 局域合成手性光场及其在分子手性探测方面的应用

3.1 合成手性场

为了产生手性效应,基于圆偏振光或是超手性光场需要同时考虑光和物质的电偶极相互作用和磁偶极相互作用(或电四极相互作用)。然而磁偶和电四相互作用一般很弱,探测信号强度往往较小,那么有没有可能只利用强的电偶极相互作用实现手性响应,合成手性光,便是这一问题的答案。不同于超手性场,合成手性光[9-15]与手性物质的相互作用在纯电偶极效应中可以产生较大的、可自由调节的对映选择性。这将从原理上给出一个全新的思路去调制光和手性分子的相互作用。另外,无论是一般的圆偏振光还是超手性场都是单频光场,手性主要体现在光场的空间分布上,而合成手性光是由多个频率的光组成的光场,其手性只与某一点的光场本身有关。

目前应用到手性探测上的合成手性光主要有双色合成手性光[88]和三色合成手性光。下面,以三色的合成手性光为例说明其产生手性效应的机制。考虑频率为 ω_1、ω_2 以及 $\omega_3\equiv\omega_1+\omega_2$ 合成的电场,有以下形式:

$$\boldsymbol{E}(t)=\boldsymbol{E}_1\mathrm{e}^{-\mathrm{i}\omega_1 t}+\boldsymbol{E}_2\mathrm{e}^{-\mathrm{i}\omega_2 t}+\boldsymbol{E}_3\mathrm{e}^{-\mathrm{i}\omega_3 t}+c.c.。\tag{9}$$

电场和分子之间的能量交换可表示为

$$\varepsilon=\int_{-\infty}^{\infty}\mathrm{d}t\boldsymbol{E}(t)\cdot\dot{\boldsymbol{P}}(t)=-2\pi\mathrm{i}\int\mathrm{d}\omega\,\omega\boldsymbol{E}(-\omega)\cdot\boldsymbol{P}(\omega),\tag{10}$$

式中，$\boldsymbol{P}(\omega)$是光场引起的诱导极化强度。考虑光场和分子的非线性相互作用，有$\boldsymbol{P}(\omega)=\boldsymbol{P}^{(1)}(\omega)+\boldsymbol{P}^{(2)}(\omega)+\cdots$，二阶非线性极化强度[86-87]可以写为

$$\boldsymbol{P}^{(2)}(\omega_3)=\varepsilon_0\chi^{(2)}(\omega_1+\omega_2)[\boldsymbol{E}(\omega_1)\times\boldsymbol{E}(\omega_2)],\tag{11a}$$

$$\boldsymbol{P}^{(2)}(\omega_2)=\varepsilon_0\chi^{(2)}(\omega_3-\omega_1)[\boldsymbol{E}(\omega_3)\times\boldsymbol{E}^{\star}(\omega_1)],\tag{11b}$$

$$\boldsymbol{P}^{(2)}(\omega_1)=\varepsilon_0\chi^{(2)}(\omega_3-\omega_2)[\boldsymbol{E}(\omega_3)\times\boldsymbol{E}^{\star}(\omega_2)],\tag{11c}$$

式中：$\chi^{(2)}$是分子朝向平均后的二阶极化率；ε_0是真空介电常数；这里式(11a)对应和频过程，而式(11b)和式(11c)对应差频过程；$\boldsymbol{E}(\omega_i)$为频率ω_i处的电场矢量的傅里叶分解；*号表示复共轭。将式(11)代入式(10)，得到二阶诱导极化对应的手性相关的能量交换[87]为

$$\varepsilon^{(2)}=4\pi\mathrm{Im}\left[-\omega_1\varepsilon_0\chi^{(2)*}(\omega_3-\omega_2)+\omega_2\varepsilon_0\chi^{(2)*}(\omega_3-\omega_1)+\omega_3\varepsilon_0\chi^{(2)*}(\omega_1+\omega_2)\right]\left\{\boldsymbol{E}^{\star}(\omega_3)\cdot\left[\boldsymbol{E}(\omega_1)\times\boldsymbol{E}(\omega_2)\right]\right\}。\tag{12}$$

定义$h^{(3)}=\boldsymbol{E}^{\star}(\omega_3)\cdot[\boldsymbol{E}(\omega_1)\times\boldsymbol{E}(\omega_2)]$为频域中最低阶手性场相关函数。只考虑电偶极相互作用，左右手分子的$\chi^{(2)}\left(\chi_{\mathrm{L}}^{(2)}=-\chi_{\mathrm{R}}^{(2)}=\chi^{(2)}\right)$互为相反数[86]，所以$\varepsilon^{(2)}$是手性依赖的$\left(\varepsilon_{\mathrm{L}}^{(2)}=-\varepsilon_{\mathrm{R}}^{(2)}=\varepsilon^{(2)}\right)$。而线性响应$P^{(1)}(\omega_i)=\tilde{\alpha}_{\mathrm{ee}}\boldsymbol{E}(\omega_i)$(不考虑磁偶影响)对应的能量交换$\varepsilon^{(1)}=-2\pi\mathrm{i}\int\mathrm{d}\omega_i\omega_i\boldsymbol{E}(-\omega_i)\cdot\boldsymbol{P}^{(1)}(\omega_i)$是手性无关的。保留到二阶非线性，则有$\varepsilon_{\mathrm{L/R}}=\varepsilon^{(1)}\pm\varepsilon^{(2)}$。对应的左右手交换能量的相对差异为

$$g\equiv 2\frac{\varepsilon_{\mathrm{L}}-\varepsilon_{\mathrm{R}}}{\varepsilon_{\mathrm{L}}+\varepsilon_{R}}\propto\frac{h^{(3)}}{|\boldsymbol{E}(\omega_1)|^2+|\boldsymbol{E}(\omega_2)|^2+|\boldsymbol{E}(\omega_3)|^2}。\tag{13}$$

我们知道不同的光学响应往往对应不同阶的非线性过程，所以对于同一个合成手性光场，可以定义不同阶的手性关联函数：

$$h^{(2n+1)}=\left\{\boldsymbol{E}(\omega_1)\cdot\left[\boldsymbol{E}(\omega_2)\times\boldsymbol{E}(\omega_3)\right]\right\}\times\left[\boldsymbol{E}(\omega_4)\cdot\boldsymbol{E}(\omega_5)\right]\cdots\left[\boldsymbol{E}(\omega_{2n})\cdot\boldsymbol{E}(\omega_{2n+1})\right]。\tag{14}$$

这里频率需要满足：

$$\omega_1+\omega_2+\cdots+\omega_{2n+1}=0,\tag{15}$$

式中，频率可以是负数，对应$\boldsymbol{E}^{*}(\omega_1)=\boldsymbol{E}(-\omega_1)$。由于手性依赖的要求，只有奇数阶的手性关联函数。对于一个多频光场来说，只要它的任意一阶手性关联函数不等于0，它就能产生只依赖电偶极相互作用的手性光学响应。这样的复合光场，就叫做合成手性光。除了频率要求以外，式(14)也对合成手性光场的偏振提出了要求：总光场的偏振不共面。

在光场手性的几何体现上，合成手性光也和其他的手性光有着很大的不同。超手性场的手性体现在电场和磁场的空间分布上，而合成手性光的手性几何体现在电场随时间演化画出来的李萨如(Lissajou)图形。如图6所示，以双色的合成手性光为例说明这个问题。在空间某一点处合成手性光的李萨如图形本身是一个三维的图形。这样一个三维的李萨如图形和它的镜面对称没办法通过平动转动等相互重合。这样的性质只和某一点处的光场本身有关而和光场的分布没有关系，所以合成手性光也被叫做局域手性场。

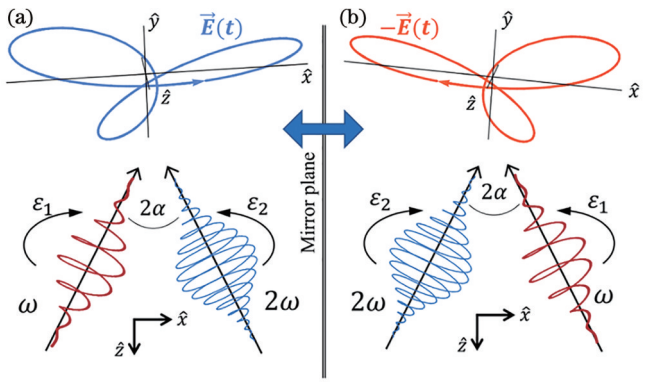

图6　合成手性光的手性体现[88]。(a)双色合成手性场的产生，图示了载波频率为ω和2ω的两个非共线波束如何产生这些场的方案。Lissajou图描述了空间中给定点中电矢量场的瞬态极化；(b)为(a)中手性场的镜像孪生图

Fig. 6　Chiral embodiment of synthetic chiral light[88]. (a) A locally chiral bichromatic electric field. Scheme illustrates how such fields are generated by two noncollinear beams of carrier frequencies ω and 2ω. Lissajou plot describes electric vector field's time-dependent polarization in a given point in space; (b) mirror twin diagram of chiral field in (a)

3.2　合成手性场在手性探测等方面的应用

双色的合成手性光主要利用强场物理的手段进行手性分子的识别。Beaulieu等[20]于2018年提供了一个束缚态手性分子动力学的灵敏时间分辨探针——光激发诱导的光电子圆二色性(PXECD)。其依赖超短圆偏振光激发的束缚电子相干螺旋运动的光激发圆二色性(PXCD)，在随机取向的手性分子集合中产生了超快速的手性响应和宏观手性密度的有效激发。通过采用线性极化激光脉冲来探测这种激发，不需要进一步的手性相互作用。并且在实验上对芬可酮分子和樟脑分子中PXECD进行了观察，通过圆极化飞秒泵浦脉冲激发对应芬可酮分子，在405 nm的线偏振探针脉冲诱导激发分子的单光子电离。如图7(a)所示，泵浦-探针PXECD信号由(L-R)图像给出，其被(L+R)/2峰值归一化，(L+R)图像反映了角度分辨光电子能谱(PES)。如预期，观察到PXECD图像的显著振幅，达

到2%，并且沿光传播方向z观察到光电子的前后不对称特征。另外，2019年Ayuso等[21]预测并数值证明了第一个仅依赖于电偶极子跃迁的具有极强手性选择性的手性高谐波(cHHG)方案，使得单个HHG谱图(单次)的手性选择性成为可能。对称性破坏导致手性介质发射的“禁止”谐波，产生巨大的、几乎无背景的手性-非手性信号，通过测量发射谐波的偏振螺旋度，可以直接检测到介质的旋向性。图7(b)所示为HHG中基于静态反射对称性破坏的手性检测结果。图7(b)左图显示了模型电位手性系综的微观y极化HHG发射，其中y极化谐波在定向平均中存活。相比之下，外消旋混合物的y极化谱为零，即y极化分量不能在方向平均中存活。图7(b)右图所示一些谐波的椭圆度达到0.5，以描述单次测量中介质的旋手性。除此之外还有光电子二色性(PECD)[90]以及其他[10,14-15,91-92]应用。更多相关研究，可以参考文献[12]。

三色合成手性光的研究主要是基于循环三能级展开。相关研究关注共振条件下的手性响应。当将光场的频率调到与分子的本征态之间共振时，分子在场中的演化将由循环三能级描述。最开始的循环三能级模

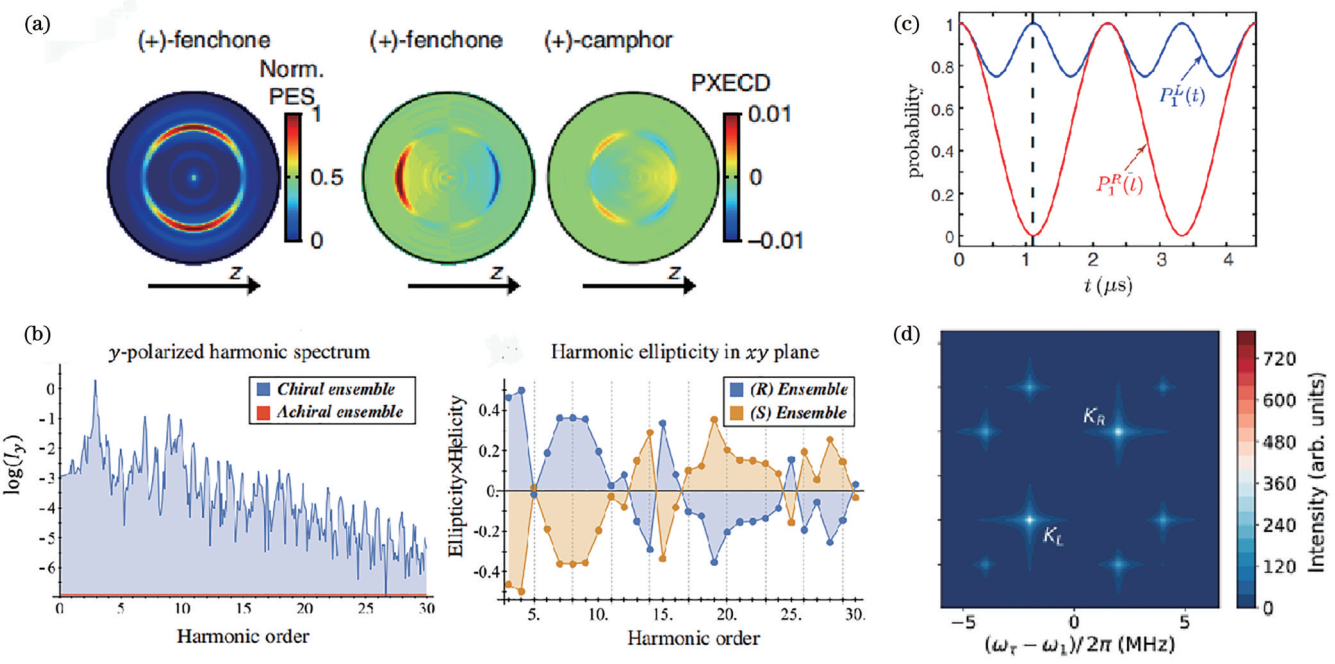

图7 合成手性场的应用。(a)(1S)-(+)-芬酮和(1R)-(+)-樟脑200 fs泵探头延迟下(L+R)图像(PES)和(L−R)图像(PXECD)的实验图像。沿光传播方向z观察到光电子的前后不对称特征[20]；(b)模型电位手性系综的微观y极化HHG发射，其中y极化谐波在定向平均中存活(左图)以及计算出的谐波椭圆率x-y平面(R)和(S)集合-螺旋度随介质的手性而变化(右图)[21]；(c)具有100%效率的内态对映体分离。左旋对映体$P_1^{\mathrm{L}}(t)$占据基态的概率用蓝线表示，右旋对映体$P_1^{\mathrm{R}}(t)$的概率用红线表示。当两个对映体的概率经历了相应的Rabi振荡的整数(1)和半整数(1/2)的周期时，在$t=\frac{\sqrt{2}\pi}{4}$ μs(黑色虚线)下实现了精确的100%效率的内态对映体分离($P_1^{\mathrm{L}}(t)=1$，$P_1^{\mathrm{R}}(t)=0$)[102]；(d)具有相等的左手和右手手性分子的外消旋混合物的二维光谱。此光谱是通过二维快速傅里叶变换获得的，并且只取变换结果的绝对值。K_{L}和K_{R}分别对应混合样品中左右手分子的ac Stark峰。通过对比峰的强度可以得到混合样品中左右手分子比例[18]

Fig. 7 Applications of synthetic chiral fields. (a) Experimental images of (L+R) image (PES) and (L−R) image (PXECD) at 200 fs pump-probe delay for (1S)-(+)-fenchone and (1R)-(+)-camphor. Characteristic forward-backward asymmetry of photoelectron is observed along light propagation direction z[20]; (b) microscopic y-polarized HHG emission from model potential chiral ensemble, where y-polarized harmonics survive orientation averaging (left picture), and calculated harmonic ellipticities in x-y plane from (R) and (S) ensembles — helicity changes with medium's chirality (right picture)[21]; (c) exactly 100%-efficiency inner-state enantioseparations. Probabilities occupying ground states of left-handed enantiomer $P_1^{\mathrm{L}}(t)$ are denoted by blue line, and those of right-handed enantiomer $P_1^{\mathrm{R}}(t)$ are denoted by red line. Exactly 100%-efficiency inner-state enantioseparations [$P_1^{\mathrm{L}}(t)=1$, $P_1^{\mathrm{R}}(t)=0$] are achieved at $t=\frac{\sqrt{2}\pi}{4}$ μs (black dashed line), when probabilities of two enantiomers experience integer (1) and half-integer (1/2) periods of their corresponding Rabi oscillations[102]; (d) two-dimensional spectra of racemic mixtures with equal left-handed and right-handed chiral molecules. These spectra are obtained through two-dimensional fast Fourier transform and only absolute value of transformation result is taken. K_{L} and K_{R} correspond to ac Stark peaks of left- and right-handed molecules in mixed sample, respectively. By comparing intensity of peaks, ratios of left- and right-handed molecules in mixed sample can be obtained[18]

型，由 Král 等[93]提出。对应的三个跃迁电偶极矩随对映体手性改变而改变符号，使手性相反的分子对相同的驱动电磁场做出不同的响应。基于循环三能级模型，人们讨论了对映体特异性状态转移[93-102]、对映体的空间分离[103-105]、手性探测[18,106-111]和对映体转化[112-117]。对映体特异性状态转移是将两个对映体从相同的初始态转移到两个不同能量的最终态。最初的对映体特异性状态转移[93]是基于缓慢的绝热过程，最近人们对对映体特异性状态转移的快速方法[94-102]感兴趣。在实现对映体特异性状态转移后，可以使用能量依赖的过程对两种对映体进行空间分离，以获得所需的对映体纯样品。例如图 7(c)所示方案[102]，当占据左旋和右旋对映异构体基态的概率同时经历其相应拉比振荡的整数(1)和半整数(1/2)周期时，不需要大失谐就可以实现 100% 效率的对映体分离[$P_1^{\mathrm{L}}(t)=1$，$P_1^{\mathrm{R}}(t)=0$，$P_1^{\mathrm{L}}(t)$、$P_1^{\mathrm{R}}(t)$分别为左旋、右旋对映体占据基态的概率]。并且由于两个对映体的演化通过改变为其相反值或选择 $\varphi=\pi$ 相互交换，也可以用 $P_1^{\mathrm{L}}(t)=0$，$P_1^{\mathrm{R}}(t)=1$ 实现精确的 100% 效率的内态对映体分离。对映体的空间分离也直接通过对映选择性光诱导场[103-105]实现。

对于手性探测，人们讨论了可以用来区分左右手的不同种类的光学响应，例如对映选择性光吸收[109]、对映选择性三波混频[118]、对映选择光折射[13,108]、对映选择 ac Stark 效应[18,111]和腔-分子混合系统的对映选择性响应[19,106-107,110]。这里以基于对映选择 ac Stark 效应的手性探测为例[18,111]：通过三个恒定的驱动场调制系统，引起这两个对映体上三个能级的不同频率位移。这样的现象不仅能反应在手性分子发光上[111]，也可以反映在二维光谱上[18]。图 7(d)所示为通过二维傅里叶变换获得的具有相等的左手和右手手性分子的外消旋混合物的二维光谱，K_{L} 和 K_{R} 分别对应混合样品中左右手分子的 ac Stark 峰。通过对比峰的强度可以得到混合样品中左右手分子比例。另外，甚至有方案讨论通过在循环三能级模型中包含的非手性电子态或振动态将手性混合物转化为纯对映体样品[18,106-111]。在实验方面，通过利用微波操作手性分子的旋转跃迁，在冷气相样品中进行了对映体特异性状态转移的原理性实验[119-121]，微波波段冷分子气体中也实现了对映选择性三波混频[122-128]。三波混谱中，两种对映体的产生信号相差 π。通过对比纯的样品的信号，可以得到待测样品的手性丰度。在微波波段操作的冷气相样品几乎不受分子退相干、多普勒效应和相位失配等这些问题的影响。这为开发新的手性检测方法[18,94,96-102,108,111,119-121]和更好地理解分子手性[129]提供了平台。

4 结 论

本文对手性光场及其在分子手性探测方面的应用进行了介绍。首先介绍了基于微纳结构增强的超手性场。其次介绍了基于超手性热点的手性分子超灵敏检测，以及基于矢量外点的超手性场增强手性光力的应用研究。然后讨论了合成手性光场的相关研究，目前主要是利用双色和三色的合成手性光进行手性分子探测，发展了光激发圆二色性、高次谐波光谱以及对映选择 ac Stark 效应等方法。另外，也基于合成手性光开展了对映体特异性状态转移等的研究。手性光场及其在分子手性探测方面的研究仍处于发展阶段。设计合理的微纳结构以实现超手性场的均匀性和更大的光学手性，是超手性场发展的挑战和关键所在。更清楚地了解超手性场与微纳结构近手性场的相互作用机制，有望提出更高精度的手性光谱方法。另外，手性光学力的使用是一个迅速发展的领域，到目前为止已经有了很多理论上的研究，在手性分离方面展现出巨大的潜力。合成手性光研究还处于起步阶段。未来我们期望能将合成手性光和微纳结构结合，发展新一代的表面增强手性光谱。

参 考 文 献

[1] Keszthelyi L. Origin of the homochirality of biomolecules[J]. Quarterly Reviews of Biophysics, 1995, 28(4): 473-507.

[2] Franks M E, MacPherson G R, Figg W D. Thalidomide[J]. The Lancet, 2004, 363(9423): 1802-1811.

[3] Kamarei F, Vajda P, Gritti F, et al. The adsorption of naproxen enantiomers on the chiral stationary phase (R, R)-whelk-O1 under supercritical fluid conditions[J]. Journal of Chromatography A, 2014, 1345: 200-206.

[4] Cordato D J, Mather L E, Herkes G K. Stereochemistry in clinical medicine: a neurological perspective[J]. Journal of Clinical Neuroscience, 2003, 10(6): 649-654.

[5] Sekhon B S. Exploiting the power of stereochemistry in drugs: an overview of racemic and enantiopure drugs[J]. Journal of Modern Medicinal Chemistry, 2013, 1(10): 10-36.

[6] Pasteur L. Sur les relations qui peuvent exister entre la forme crystalline, la composition chimique et le sens de la polarization rotatoire[J]. Annales de Chimie et de Physique, 1848, 24: 442-459.

[7] Tang Y Q, Cohen A E. Optical chirality and its interaction with matter[J]. Physical Review Letters, 2010, 104(16): 163901.

[8] Forbes K A, Andrews D L. Optical orbital angular momentum: twisted light and chirality[J]. Optics Letters, 2018, 43(3): 435-438.

[9] Ayuso D, Neufeld O, Ordonez A F, et al. Synthetic chiral light for efficient control of chiral light-matter interaction[J]. Nature Photonics, 2019, 13: 866-871.

[10] Ayuso D, Ordonez A F, Decleva P, et al. Enantio-sensitive unidirectional light bending[J]. Nature Communications, 2021, 12: 3951.

[11] Ayuso D, Ordonez A F, Ivanov M, et al. Ultrafast optical rotation in chiral molecules with ultrashort and tightly focused beams[J]. Optica, 2021, 8(10): 1243-1246.

[12] Ayuso D, Ordonez A F, Smirnova O. Ultrafast chirality: the road to efficient chiral measurements[J]. Physical Chemistry Chemical Physics: PCCP, 2022, 24(44): 26962-26991.

[13] Khokhlova M, Pisanty E, Patchkovskii S, et al. Enantiosensitive steering of free-induction decay[J]. Science Advances, 2022, 8(24): eabq1962.

[14] Neufeld O, Hübener H, Rubio A, et al. Strong chiral dichroism

and enantiopurification in above-threshold ionization with locally chiral light[J]. Physical Review Research, 2021, 3(3): L032006.

[15] Neufeld O, Wengrowicz O, Peleg O, et al. Detecting multiple chiral centers in chiral molecules with high harmonic generation [J]. Optics Express, 2022, 30(3): 3729-3740.

[16] Forbes K A. Raman optical activity using twisted photons[J]. Physical Review Letters, 2019, 122(10): 103201.

[17] Forbes K A, Jones G A. Optical vortex dichroism in chiral particles[J]. Physical Review A, 2021, 103(5): 053515.

[18] Cai M R, Ye C, Dong H, et al. Enantiodetection of chiral molecules via two-dimensional spectroscopy[J]. Physical Review Letters, 2022, 129(10): 103201.

[19] Ye C, Sun Y F, Li Y, et al. Single-shot nondestructive quantum sensing for gaseous samples with hundreds of chiral molecules[J]. The Journal of Physical Chemistry Letters, 2023, 14(30): 6772-6777.

[20] Beaulieu S, Comby A, Descamps D, et al. Photoexcitation circular dichroism in chiral molecules[J]. Nature Physics, 2018, 14: 484-489.

[21] Neufeld O, Ayuso D, Decleva P, et al. Ultrasensitive chiral spectroscopy by dynamical symmetry breaking in high harmonic generation[J]. Physical Review X, 2019, 9(3): 031002.

[22] Govorov A O. Plasmon-induced circular dichroism of a chiral molecule in the vicinity of metal nanocrystals. application to various geometries[J]. The Journal of Physical Chemistry C, 2011, 115(16): 7914-7923.

[23] Wang R Y, Wang P, Liu Y, et al. Experimental observation of giant chiroptical amplification of small chiral molecules by gold nanosphere clusters[J]. The Journal of Physical Chemistry C, 2014, 118(18): 9690-9695.

[24] Wu T, Zhang W X, Wang R Y, et al. A giant chiroptical effect caused by the electric quadrupole[J]. Nanoscale, 2017, 9(16): 5110-5118.

[25] Wu T, Ren J, Wang R Y, et al. Competition of chiroptical effect caused by nanostructure and chiral molecules[J]. The Journal of Physical Chemistry C, 2014, 118(35): 20529-20537.

[26] Wu T, Zhang X H, Wang R Y, et al. Strongly enhanced Raman optical activity in molecules by magnetic response of nanoparticles[J]. The Journal of Physical Chemistry C, 2016, 120(27): 14795-14804.

[27] Lipkin D M. Existence of a new conservation law in electromagnetic theory[J]. Journal of Mathematical Physics, 1964, 5(5): 696-700.

[28] 芮光浩, 詹其文. 基于纳米光子学的手性检测与表征技术(特邀)[J]. 光子学报, 2022, 51(5): 0551301.
Rui G H, Zhan Q W. Nanophotonic methods for chiral sensing and characterization (invited)[J]. Acta Photonica Sinica, 2022, 51(5): 0551301.

[29] Harris R A. On the optical rotary dispersion of polymers[J]. The Journal of Chemical Physics, 1965, 43(3): 959-970.

[30] Valev V K, Baumberg J J, Sibilia C, et al. Chirality and chiroptical effects in plasmonic nanostructures: fundamentals, recent progress, and outlook[J]. Advanced Materials, 2013, 25 (18): 2517-2534.

[31] Liu Y, Hou S S, Zhang W X, et al. Tunable manipulation of enantiomers by vector exceptional points[J]. The Journal of Physical Chemistry C, 2022, 126(6): 3127-3133.

[32] Liu Y, Zhang W X, He L, et al. All-optical separation of chiral nanoparticles on silicon-based microfluidic chips with vector exceptional points[J]. APL Photonics, 2023, 8(3): 036112.

[33] Zhang W X, Wu T, Wang R Y, et al. Surface-enhanced circular dichroism of oriented chiral molecules by plasmonic nanostructures[J]. The Journal of Physical Chemistry C, 2017, 121(1): 666-675.

[34] 张慧珍, 张蔚暄, 侯赛赛, 等. 表面增强的手性分子光谱研究进展[J]. 中国科学: 物理学 力学 天文学, 2020, 50(9): 48-69.
Zhang H Z, Zhang W X, Hou S S, et al. Recent research progress on surface-enhanced spectra of chiral molecules[J]. Scientia Sinica (Physica, Mechanica & Astronomica), 2020, 50 (9): 48-69.

[35] Zhang H Z, Zhang A Z, Hou S S, et al. Superchiral fields generated by nanostructures and their applications for chiral sensing[J]. Chinese Physics B, 2021, 30(11): 113303.

[36] Hendry E, Carpy T, Johnston J, et al. Ultrasensitive detection and characterization of biomolecules using superchiral fields[J]. Nature Nanotechnology, 2010, 5(11): 783-787.

[37] Schäferling M, Dregely D, Hentschel M, et al. Tailoring enhanced optical chirality: design principles for chiral plasmonic nanostructures[J]. Physical Review X, 2012, 2(3): 031010.

[38] Meinzer N, Hendry E, Barnes W L. Probing the chiral nature of electromagnetic fields surrounding plasmonic nanostructures[J]. Physical Review B, 2013, 88(4): 041407.

[39] García-Etxarri A, Dionne J A. Surface-enhanced circular dichroism spectroscopy mediated by nonchiral nanoantennas[J]. Physical Review B, 2013, 87(23): 235409.

[40] Cao H, Wiersig J. Dielectric microcavities: model systems for wave chaos and non-Hermitian physics[J]. Reviews of Modern Physics, 2015, 87(1): 61-111.

[41] García-Etxarri A, Gómez-Medina R, Froufe-Pérez L S, et al. Strong magnetic response of submicron silicon particles in the infrared[J]. Optics Express, 2011, 19(6): 4815-4826.

[42] Yao K, Liu Y M. Enhancing circular dichroism by chiral hotspots in silicon nanocube dimers[J]. Nanoscale, 2018, 10 (18): 8779-8786.

[43] Liu Y, Zhao W, Ji Y, et al. Strong superchiral field in hot spots and its interaction with chiral molecules[J]. Europhysics Letters, 2015, 110(1): 17008.

[44] Zhao X, Reinhard B M. Switchable chiroptical hot-spots in silicon nanodisk dimers[J]. ACS Photonics, 2019, 6(8): 1981-1989.

[45] Alizadeh M H, Reinhard B M. Plasmonically enhanced chiral optical fields and forces in achiral split ring resonators[J]. ACS Photonics, 2015, 2(3): 361-368.

[46] Wu T, Zhang W X, Zhang H Z, et al. Vector exceptional points with strong superchiral fields[J]. Physical Review Letters, 2020, 124(8): 083901.

[47] Yoo S, Cho M, Park Q H. Globally enhanced chiral field generation by negative-index metamaterials[J]. Physical Review B, 2014, 89(16): 161406.

[48] Zhang H Z, Zhang W X, Chen S H, et al. Experimental observation of vector bound states in the continuum[J]. Advanced Optical Materials, 2023, 11(12): 2203118.

[49] Auguié B, Alonso-Gómez J L, Guerrero-Martínez A, et al. Fingers crossed: optical activity of a chiral dimer of plasmonic nanorods[J]. The Journal of Physical Chemistry Letters, 2011, 2 (8): 846-851.

[50] Lieberman I, Shemer G, Fried T, et al. Plasmon-resonance-enhanced absorption and circular dichroism[J]. Angewandte Chemie International Edition, 2008, 47(26): 4855-4857.

[51] Layani M E, Ben M A, Varenik M, et al. Chiroptical activity in silver cholate nanostructures induced by the formation of nanoparticle assemblies[J]. The Journal of Physical Chemistry C, 2013, 117(43): 22240-22244.

[52] di Gregorio M C, Ben Moshe A, Tirosh E, et al. Chiroptical study of plasmon-molecule interaction: the case of interaction of glutathione with silver nanocubes[J]. The Journal of Physical Chemistry C, 2015, 119(30): 17111-17116.

[53] Govorov A O, Fan Z, Hernandez P, et al. Theory of circular dichroism of nanomaterials comprising chiral molecules and nanocrystals: plasmon enhancement, dipole interactions, and dielectric effects [J]. Nano letters, 2010, 10(4): 1374-82.

[54] Brullot W, Vanbel M K, Swusten T, et al. Resolving enantiomers using the optical angular momentum of twisted light

[J]. Science Advances, 2016, 2(3): e1501349.
[55] Levi-Belenkova T, Govorov A O, Markovich G. Orientation-sensitive peptide-induced plasmonic circular dichroism in silver nanocubes[J]. The Journal of Physical Chemistry C, 2016, 120(23): 12751-12756.
[56] Luber S, Herrmann C, Reiher M. Relevance of the electric-dipole: electric-quadrupole contribution to Raman optical activity spectra[J]. The Journal of Physical Chemistry B, 2008, 112(7): 2218-2232.
[57] Alexandrescu A, Cojoc D, di Fabrizio E. Mechanism of angular momentum exchange between molecules and Laguerre-Gaussian beams[J]. Physical Review Letters, 2006, 96(24): 243001.
[58] Andrews D L, Romero L C D, Babiker M. On optical vortex interactions with chiral matter[J]. Optics Communications, 2004, 237(1/2/3): 133-139.
[59] Babiker M, Bennett C R, Andrews D L, et al. Orbital angular momentum exchange in the interaction of twisted light with molecules[J]. Physical Review Letters, 2002, 89(14): 143601.
[60] Jáuregui R. Rotational effects of twisted light on atoms beyond the paraxial approximation[J]. Physical Review A, 2004, 70(3): 033415.
[61] Mondal P K, Deb B, Majumder S. Angular momentum transfer in interaction of Laguerre-Gaussian beams with atoms and molecules[J]. Physical Review A, 2014, 89(6): 063418.
[62] Romero L C D, Andrews D L, Babiker M. A quantum electrodynamics framework for the nonlinear optics of twisted beams[J]. Journal of Optics B: Quantum and Semiclassical Optics, 2002, 4(2): S66-S72.
[63] Wu T, Wang R Y, Zhang X D. Plasmon-induced strong interaction between chiral molecules and orbital angular momentum of light[J]. Scientific Reports, 2015, 5: 18003.
[64] Abdali S, Blanch E W. Surface enhanced Raman optical activity (SEROA)[J]. Chemical Society Reviews, 2008, 37(5): 980-992.
[65] Efrima S. Raman optical activity of molecules adsorbed on metal surfaces: theory[J]. The Journal of Chemical Physics, 1985, 83(3): 1356-1362.
[66] Zhang W X, Wu T, Wang R Y, et al. Amplification of the molecular chiroptical effect by low-loss dielectric nanoantennas [J]. Nanoscale, 2017, 9(17): 5701-5707.
[67] Bhardwaj A, Kaur J, Wuest M, et al. In situ click chemistry generation of cyclooxygenase-2 inhibitors[J]. Nature Communications, 2017, 8(1): 1.
[68] Kakkar T, Keijzer C, Rodier M, et al. Superchiral near fields detect virus structure[J]. Light, Science & Applications, 2020, 9(1): 195.
[69] Li J G, Wang M S, Wu Z L, et al. Tunable chiral optics in all-solid-phase reconfigurable dielectric nanostructures[J]. Nano Letters, 2021, 21(2): 973-979.
[70] Rodier M, Keijzer C, Milner J, et al. Probing specificity of protein-protein interactions with chiral plasmonic nanostructures [J]. The Journal of Physical Chemistry Letters, 2019, 10(20): 6105-6111.
[71] Tullius R, Karimullah A S, Rodier M, et al. "superchiral" spectroscopy: detection of protein higher order hierarchical structure with chiral plasmonic nanostructures[J]. Journal of the American Chemical Society, 2015, 137(26): 8380-8383.
[72] Tullius R, Platt G W, Khorashad L K, et al. Superchiral plasmonic phase sensitivity for fingerprinting of protein interface structure[J]. ACS Nano, 2017, 11(12): 12049-12056.
[73] Zhang H, Govorov A O. Giant circular dichroism of a molecule in a region of strong plasmon resonances between two neighboring gold nanocrystals [J]. Physical Review B, 2013, 87(7): 075410.
[74] Bradshaw D S, Andrews D L. Laser optical separation of chiral molecules[J]. Optics Letters, 2015, 40(4): 677-680.
[75] Canaguier-Durand A, Hutchison J A, Genet C, et al. Mechanical separation of chiral dipoles by chiral light[J]. New Journal of Physics, 2013, 15(12): 123037.
[76] Hayat A, Mueller J P, Capasso F. Lateral chirality-sorting optical forces[J]. Proceedings of the National Academy of Sciences of the United States of America, 2015, 112(43): 13190-13194.
[77] Pellegrini G, Finazzi M, Celebrano M, et al. Superchiral Surface Waves for All-Optical Enantiomer Separation [J]. The Journal of Physical Chemistry C, 2019, 123(46): 28336-42.
[78] Soltani M, Lin J, Forties R A, et al. Nanophotonic trapping for precise manipulation of biomolecular arrays[J]. Nature Nanotechnology, 2014, 9: 448-452.
[79] Tkachenko G, Brasselet E. Optofluidic sorting of material chirality by chiral light[J]. Nature Communications, 2014, 5: 3577.
[80] Wang S B, Chan C T. Lateral optical force on chiral particles near a surface[J]. Nature Communications, 2014, 5: 3307.
[81] Fang L, Wang J. Optical trapping separation of chiral nanoparticles by subwavelength slot waveguides[J]. Physical Review Letters, 2021, 127(23): 233902.
[82] Shoji T, Tsuboi Y. Plasmonic optical tweezers toward molecular manipulation: tailoring plasmonic nanostructure, light source, and resonant trapping[J]. The Journal of Physical Chemistry Letters, 2014, 5(17): 2957-2967.
[83] Hou S S, Liu Y, Zhang W X, et al. Separating and trapping of chiral nanoparticles with dielectric photonic crystal slabs[J]. Optics Express, 2021, 29(10): 15177-15189.
[84] Lin Z H, Zhang J W, Huang J S. Plasmonic elliptical nanoholes for chiroptical analysis and enantioselective optical trapping[J]. Nanoscale, 2021, 13(20): 9185-9192.
[85] Zhao Y, Saleh A A E, Dionne J A. Enantioselective optical trapping of chiral nanoparticles with plasmonic tweezers[J]. ACS Photonics, 2016, 3(3): 304-309.
[86] Fischer P, Hache F. Nonlinear optical spectroscopy of chiral molecules[J]. Chirality, 2005, 17(8): 421-437.
[87] Giordmaine J A. Nonlinear optical properties of liquids[J]. Physical Review, 1965, 138(6A): A1599-A1606.
[88] Neufeld O, Tzur M E, Cohen O. Degree of chirality of electromagnetic fields and maximally chiral light[J]. Physical Review A, 2020, 101(5): 053831.
[89] Zhao Y, Saleh A A, Dionne J A. Enantioselective optical trapping of chiral nanoparticles with plasmonic tweezers [J]. Acs Photonics, 2016, 3(3): 304-9.
[90] Bloch E, Larroque S, Rozen S, et al. Revealing the influence of molecular chirality on tunnel-ionization dynamics[J]. Physical Review X, 2021, 11(4): 041056.
[91] Ayuso D. New opportunities for ultrafast and highly enantio-sensitive imaging of chiral nuclear dynamics enabled by synthetic chiral light[J]. Physical Chemistry Chemical Physics, 2022, 24(17): 10193-10200.
[92] Ayuso D, Ordonez A, Ivanov M, et al. Ultrafast optical rotation in chiral molecules with ultrashort and tightly focused beams[C]//OSA Nonlinear Optics 2021, August 9-13, 2021, Washington, DC. Washington, DC: Optica Publishing Group, 2021: NW2A.2.
[93] Král P, Shapiro M. Cyclic population transfer in quantum systems with broken symmetry[J]. Physical Review Letters, 2001, 87(18): 183002.
[94] Leibscher M, Kalveram J, Koch C P. Rational pulse design for enantiomer-selective microwave three-wave mixing[J]. Symmetry, 2022, 14(5): 871.
[95] Li Y, Bruder C. Dynamic method to distinguish between left- and right-handed chiral molecules[J]. Physical Review A, 2008, 77(1): 015403.
[96] Liu B, Ye C, Sun C P, et al. Enantiospecific state transfer for gaseous symmetric-top chiral molecules[J]. Physical Review A, 2022, 105(4): 043110.

[97] Torosov B T, Drewsen M, Vitanov N V. Efficient and robust chiral resolution by composite pulses [J]. Physical Review A, 2020, 101(6): 063401.

[98] Torosov B T, Michael D, Vitanov Nikolay V. Chiral resolution by composite Raman pulses[J]. Physical Review Research, 2020, 2(4): 043235.

[99] Vitanov N V, Drewsen M. Highly efficient detection and separation of chiral molecules through shortcuts to adiabaticity [J]. Physical Review Letters, 2019, 122(17): 173202.

[100] Wu J L, Wang Y, Han J X, et al. Two-path interference for enantiomer-selective state transfer of chiral molecules[J]. Physical Review Applied, 2020, 13(4): 044021.

[101] Wu J L, Wang Y, Song J, et al. Robust and highly efficient discrimination of chiral molecules through three-mode parallel paths[J]. Physical Review A, 2019, 100(4): 043413.

[102] Ye C, Zhang Q S, Chen Y Y, et al. Effective two-level models for highly efficient inner-state enantioseparation based on cyclic three-level systems of chiral molecules[J]. Physical Review A, 2019, 100(4): 043403.

[103] Li X, Shapiro M. Theory of the optical spatial separation of racemic mixtures of chiral molecules[J]. The Journal of Chemical Physics, 2010, 132(19): 194315.

[104] Li Y, Bruder C, Sun C P. Generalized Stern-Gerlach effect for chiral molecules[J]. Physical Review Letters, 2007, 99(13): 130403.

[105] Liu B, Ye C, Sun C P, et al. Spatial enantioseparation of gaseous chiral molecules[J]. Physical Review A, 2021, 104(1): 013113.

[106] Chen Y Y, Cheng J J, Ye C, et al. Enantiodetection of cyclic three-level chiral molecules in a driven cavity[J]. Physical Review Research, 2022, 4(1): 013100.

[107] Chen Y Y, Ye C, Li Y. Enantio-detection via cavity-assisted three-photon processes[J]. Optics Express, 2021, 29(22): 36132-36144.

[108] Chen Y Y, Ye C, Zhang Q S, et al. Enantio-discrimination via light deflection effect[J]. The Journal of Chemical Physics, 2020, 152(20): 204305.

[109] Jia W Z, Wei L F. Probing molecular chirality by coherent optical absorption spectra[J]. Physical Review A, 2011, 84(5): 053849

[110] Kang Y H, Shi Z C, Song J, et al. Effective discrimination of chiral molecules in a cavity[J]. Optics Letters, 2020, 45(17): 4952-4955.

[111] Ye C, Zhang Q S, Chen Y Y, et al. Determination of enantiomeric excess with chirality-dependent ac Stark effects in cyclic three-level models[J]. Physical Review A, 2019, 100(3): 033411.

[112] Brumer P, Frishman E, Shapiro M. Principles of electric-dipole-allowed optical control of molecular chirality[J]. Physical Review A, 2001, 65(1): 015401.

[113] Gerbasi D, Shapiro M, Brumer P. Theory of enantiomeric control in dimethylallene using achiral light[J]. The Journal of Chemical Physics, 2001, 115(12): 5349-5352.

[114] Král P, Thanopulos I, Shapiro M, et al. Two-step enantio-selective optical switch[J]. Physical Review Letters, 2003, 90(3): 033001.

[115] Shapiro M, Frishman E, Brumer P. Coherently controlled asymmetric synthesis with achiral light[J]. Physical Review Letters, 2000, 84(8): 1669-1672.

[116] Ye C, Liu B, Chen Y Y, et al. Enantio-conversion of chiral mixtures via optical pumping[J]. Physical Review A, 2021, 103(2): 022830.

[117] Ye C, Zhang Q S, Chen Y Y, et al. Fast enantioconversion of chiral mixtures based on a four-level double-Δ model[J]. Physical Review Research, 2020, 2(3): 033064.

[118] Hirota E. Triple resonance for a three-level system of a chiral molecule[J]. Proceedings of the Japan Academy: Series B, Physical and Biological Sciences, 2012, 88(3): 120-128.

[119] Eibenberger S, Doyle J, Patterson D. Enantiomer-specific state transfer of chiral molecules[J]. Physical Review Letters, 2017, 118(12): 123002.

[120] Lee J, Bischoff J, Hernandez-Castillo A O, et al. Quantitative study of enantiomer-specific state transfer[J]. Physical Review Letters, 2022, 128(17): 173001.

[121] Pérez C, Steber A L, Domingos S R, et al. Coherent enantiomer-selective population enrichment using tailored microwave fields[J]. Angewandte Chemie (International Ed. in English), 2017, 56(41): 12512-12517.

[122] Lobsiger S, Perez C, Evangelisti L, et al. Molecular structure and chirality detection by Fourier transform microwave spectroscopy[J]. The Journal of Physical Chemistry Letters, 2015, 6(1): 196-200.

[123] Patterson D, Doyle J M. Sensitive chiral analysis via microwave three-wave mixing[J]. Physical Review Letters, 2013, 111(2): 023008.

[124] Patterson D, Schnell M. New studies on molecular chirality in the gas phase: enantiomer differentiation and determination of enantiomeric excess[J]. Physical Chemistry Chemical Physics: PCCP, 2014, 16(23): 11114-11123.

[125] Patterson D, Schnell M, Doyle J M. Enantiomer-specific detection of chiral molecules via microwave spectroscopy[J]. Nature, 2013, 497(7450): 475-477.

[126] Shubert V A, Schmitz D, Medcraft C, et al. Rotational spectroscopy and three-wave mixing of 4-carvomenthenol: a technical guide to measuring chirality in the microwave regime[J]. The Journal of Chemical Physics, 2015, 142(21): 214201.

[127] Shubert V A, Schmitz D, Patterson D, et al. Identifying enantiomers in mixtures of chiral molecules with broadband microwave spectroscopy[J]. Angewandte Chemie (International Ed. in English), 2014, 53(4): 1152-1155.

[128] Shubert V A, Schmitz D, Pérez C, et al. Chiral analysis using broadband rotational spectroscopy[J]. The Journal of Physical Chemistry Letters, 2016, 7(2): 341-350.

[129] Sun W H, Tikhonov D S, Singh H, et al. Inducing transient enantiomeric excess in a molecular quantum racemic mixture with microwave fields[J]. Nature Communications, 2023, 14: 934.

Chiral Light Field and Its Recent Research Progress in Molecular Chirality Detection (Invited)

Mu Xiaowei, Ye Chong**, Zhang Xiangdong*

School of Physics, Beijing Institute of Technology, Beijing 100081, *China*

Abstract

Significance Chirality is a property of an object that cannot be superimposed on its mirror image by translation or rotation operations. The two enantiomers of chiral molecules have the same physical properties but completely different chemical properties. Therefore, effective detection and characterization of chiral molecules are crucial for such fields as pharmaceuticals and biochemistry. Chiral objects exhibit optical activity, and the optical chirality response generated during the interaction with other chiral objects provides a basic strategy for effective enantiomer identification. The light field plays a vital role in the detection of chiral molecules, and according to Curie's asymmetry principle, the chiral response often requires a chiral light field. The light field chirality greatly affects the optical response intensity of chiral media. Therefore, how to enhance the chirality of ordinary light fields is a core issue in chirality research. The circularly polarized light field is the most common type of chiral light, playing an important part in chiral responses such as optical rotation, circular dichroism, and Raman optical activity. However, the chiral response generated by circularly polarized light fields is often weak, which greatly affects the ability of these methods to detect molecular chirality. Therefore, many other optical fields have been proposed, such as superchiral field, optical field with orbital angular momentum, and synthetic chiral light.

Progress Currently, extensive theoretical and experimental research has been conducted on the regulation of chiral light fields and their ultra-sensitive detection with the assistance of artificial nanostructures. After the concept of optical chirality (C) was proposed, its physical meaning was improved by Tang and Cohen. By employing the expression of optical chirality, when the optical chirality of a certain light field is greater than that of circularly polarized light, it is called superchiral field. When chiral structures are adopted for chiral detection, the chiral signals of molecules are often influenced by the chiral signal of the structure itself (Fig. 1). To this end, it is proposed that non-chiral structures should be utilized to generate superchiral fields for enhanced spectral detection, such as the study of nanostructure superchiral hotspots, and the construction of vector exceptional points (EPs) and Bound states in the continuum (BICs) to generate strong and uniform superchiral field over a large area, which has been experimentally validated (Fig. 2). In molecular chirality ultra-sensitive detection based on superchiral field, the initial research mostly focuses on enhancing the circular dichroism signal of molecules by obtaining superchiral hotspots with enhanced chirality density (Fig. 3). Initially, it was believed that the significant enhancement of chiral signals by placing molecules in hotspots was due to the enhanced field strength at the hotspots. Later, it was theoretically proven that the peak/valley intensity of plasma-induced circular dichroism enhancement directly corresponds to a larger optical chirality in the near-field, rather than a larger enhanced electromagnetic field intensity at the hotspots (Fig. 4). Additionally, the interaction between orbital angular momentum beams and chiral molecules has been extensively discussed. Placing chiral molecules in the hotspots of dimers can observe a significant enhancement effect of chiral signals (Fig. 3). The study of employing dielectric nanoparticles to enhance molecular Raman optical activity (ROA) signals can provide more comprehensive information on molecular chirality structures, and also investigate the thermal effects of dielectric and metal structures under light irradiation (Fig. 4). Meanwhile, the strength of chiral optical gradient force is related to the gradient of optical field chirality. The utilization of a superchiral field can increase the total optical force difference of enantiomers, achieving the separation of enantiomers and nanoparticles (Fig. 5). Research based on circularly polarized light or superchiral light fields requires consideration of both electric dipole interactions and magnetic dipole interactions (or electric quadrupole interactions) between light and matter. However, the interaction between magnetic dipoles and electric quadrupoles is usually weak, with often small detection signal strength. The interaction between synthetic chiral light and chiral substances can generate significant and freely adjustable enantioselectivity in pure electric dipole effects. Synthetic chiral light is a light field composed of multiple light frequencies, which requires that the polarization of the total light field should not be coplanar, and its chirality is only related to the light field itself at a certain point (Fig. 6). The synthesis of dual color chiral light mainly employs strong field physics to recognize chiral molecules, such as photoexcited circular dichroism (PXCD) and high harmonic generation (HHG) spectroscopy. The research on the tricolor synthesis of chiral light is mainly based on the cyclic three-level model, and researchers have discussed enantiomer specific state transfer (ESST) and enantiomer spatial separation. For chiral

detection, different types of optical responses that can be adopted to distinguish left and right hands have been discussed, such as enantioselective light absorption, enantioselective three-wave mixing, enantioselective ac Stark effect, and enantioselective response of cavity molecule mixing systems (Fig. 7).

Conclusions and Prospects We introduce chiral light fields and their applications in molecular chirality detection. Firstly, we present the enhancement of superchiral fields based on nanostructures and review their applications in two aspects, including chiral molecule ultra-sensitive detection based on superchiral hotspots and chiral optical force enhancement based on vector exceptional points. Then the relevant research on synthetic chiral light is discussed. Currently, the main focus is on the detection of chiral molecules using bicolor and tricolor synthetic chiral light. Meanwhile, we have developed methods such as photoexcited circular dichroism, high harmonic generation spectroscopy, and enantioselective ac Stark effect. In addition, research on ESST has also been conducted based on synthetic chiral light. The research on the chiral light field and its applications in molecular chirality detection is still in the development stage. Thus, designing reasonable nanostructures to achieve uniformity and higher optical chirality C in the development of superchiral fields is a challenge and key. A clearer understanding of the interaction mechanism between the superchiral field and the near chiral field of nanostructures can potentially boost the development of higher-precision chiral spectroscopy methods. In addition, the utilization of chiral optical forces is a rapidly developing field where there have been many theoretical studies so far, demonstrating enormous potential in chiral separation. The research on synthetic chiral light is still in its early stage. In the future, we hope to combine synthetic chiral light with nanostructures to develop a new generation of surface-enhanced chiral light.

Key words micro nano optics; superchiral field; synthetic chiral light